A&A 620, A99 (2018)
https://doi.org/10.1051/0004-6361/201833263

Astronomy & Astrophysics

The effect of metallicity on Cepheid period-luminosity relations from a Baade-Wesselink analysis of Cepheids in the Milky Way and Magellanic Clouds⋆,⋆⋆

W. Gieren[1,2], J. Storm[3], P. Konorski[4], M. Górski[1,2], B. Pilecki[5], I. Thompson[6], G. Pietrzyński[5,1], D. Graczyk[1,2,5], T. G. Barnes[7], P. Fouqué[8,9], N. Nardetto[10], A. Gallenne[11], P. Karczmarek[4], K. Suchomska[4], P. Wielgórski[5], M. Taormina[5], and B. Zgirski[5]

[1] Universidad de Concepción, Departamento Astronomía, Casilla 160-C, Concepción, Chile
e-mail: wgieren@astro-udec.cl
[2] Millenium Institute of Astrophysics, Santiago, Chile
[3] Leibniz-Institut für Astrophysik Potsdam (AIP), An der Sternwarte 16, 14482 Potsdam, Germany
[4] Obserwatorium Astronomiczne, Uniwersytet Warszawski, Al. Ujazdowskie 4, 00-478 Warsaw, Poland
[5] Centrum Astronomiczne im. Mikołaja Kopernika (CAMK), PAN, Bartycka 18, 00-716 Warsaw, Poland
[6] Carnegie Observatories, 813 Santa Barbara Street, Pasadena, CA 911101-1292, USA
[7] University of Texas at Austin, McDonald Observatory, 1 University Station, C1402, Austin, TX 78712-0259, USA
[8] IRAP, Université de Toulouse, CNRS, 14 av. E. Belin, 31400 Toulouse, France
[9] CFHT Corporation, 65-1238 Mamalahoa Hwy, Kamuela, HI 96743, USA
[10] Université Côte d'Azur, Observatoire de la Côte d'Azur, CNRS, Laboratoire Lagrange, France
[11] European Southern Observatory, Alonso de Córdova 3107, Casilla 19001, Santiago, Chile

Received 19 April 2018 / Accepted 7 September 2018

ABSTRACT

Context. The extragalactic distance scale builds on the Cepheid period-luminosity (PL) relation. Decades of work have not yet convincingly established the sensitivity of the PL relation to metallicity. This currently prevents a determination of the Hubble constant accurate to 1% from the classical Cepheid-SN Ia method.
Aims. In this paper we carry out a strictly differential comparison of the absolute PL relations obeyed by classical Cepheids in the Milky Way (MW), LMC, and SMC galaxies. Taking advantage of the substantial metallicity difference among the Cepheid populations in these three galaxies, we want to establish a possible systematic trend of the PL relation absolute zero point as a function of metallicity, and to determine the size of such an effect in the optical and near-infrared photometric bands.
Methods. We used a IRSB Baade-Wesselink-type method to determine individual distances to the Cepheids in our samples in the MW, LMC, and SMC. For our analysis, we used a greatly enhanced sample of Cepheids in the SMC (31 stars) compared to the small sample (5 stars) available in our previous work. We used the distances to determine absolute Cepheid PL relations in the optical and near-infrared bands in each of the three galaxies.
Results. Our distance analysis of 31 SMC Cepheids with periods of 4–69 days yields tight PL relations in all studied bands, with slopes consistent with the corresponding LMC and MW relations. Adopting the very accurately determined LMC slopes for the optical and near-infrared bands, we determine the zero point offsets between the corresponding absolute PL relations in the three galaxies.
Conclusions. We find that in all bands the metal-poor SMC Cepheids are intrinsically fainter than their more metal-rich counterparts in the LMC and MW. In the K band the metallicity effect is -0.23 ± 0.06 mag dex^{-1}, while in the $V,(V-I)$ Wesenheit index it is slightly stronger, -0.34 ± 0.06 mag dex^{-1}. We find suggestive evidence that the metallicity sensitivity of the PL relation might be nonlinear, being small in the range between solar and LMC Cepheid metallicity, and becoming steeper towards the lower-metallicity regime.

Key words. stars: variables: Cepheids – stars: distances – stars: fundamental parameters – Magellanic Clouds – galaxies: distances and redshifts

1. Introduction

One of the most important current challenges in astrophysics is the quest for a 1% determination of the local value of the Hubble constant H_0. The traditional route to determine the value of the local Hubble constant is to use reddening insensitive photometric observations of classical Cepheid variables in nearby type Ia supernovae (SN Ia) host galaxies (e.g., Freedman et al. 2001; Sandage et al. 2006; and references therein). The distances to these galaxies can then be determined from the Cepheid period-luminosity (PL) relation, calibrating in this way the SN Ia peak luminosities. The most recent application of this method has led to an accuracy of H_0 of 2.4% (Riess et al. 2016, 2018).

It is obviously of fundamental importance in this process to provide a very accurate absolute calibration of the Cepheid PL

⋆ Based on data obtained with ESO-LP-190.D-0237, and programs 097.D-0150 and 097.D-0151.
⋆⋆ Full Tables 2, 4, and B.1 are only available at the CDS via anonymous ftp to cdsarc.u-strasbg.fr (130.79.128.5) or via http://cdsarc.u-strasbg.fr/viz-bin/qcat?J/A+A/620/A99

relation. This can be achieved in different ways, using Cepheids in our own Galaxy that have accurate parallax measurements, or using extragalactic Cepheids for which the distances of their host galaxies have been very accurately determined with some Cepheid-independent method. A critical aspect of the calibration of the PL relation is a precise determination of its possible dependence on the metallicity of the Cepheid variables. Without an accurate knowledge of this "metallicity effect" a distance measurement to a galaxy accurate to 1% with a Cepheid PL relation is clearly not possible. In the past a lot of work was done with a variety of methods to determine the metallicity dependence of the Cepheid PL relation. Early work includes the studies of Gould (1994), Kennicutt et al. (1998), and Sakai et al. (2004). More recent studies on the metallicity effect are those of Shappee & Stanek (2011), Mager et al. (2013), and Fausnaugh et al. (2015), among others. A very detailed compilation of metallicity effect determinations prior to 2008 can be found in Table 1 of Romaniello et al. (2008). These studies seem to indicate that the metallicity effect in the near-infrared JHK bands is small, perhaps even vanishing, while there is a significant effect in optical and mid-infrared photometric bands (e.g., Freedman & Madore 2011). While most studies yielded a negative sign of the metallicity effect in optical bands meaning that more metal-rich Cepheids are intrinsically brighter than their more metal-poor counterparts of the same pulsation period, the work of Romaniello et al. (2008) has yielded the opposite sign for the effect in the V band, meaning that metal-poor Cepheids are intrinsically brighter than their more metal-rich counterparts of the same pulsation period. Theoretical studies (e.g., Caputo et al. 2000; Bono et al. 2008) appear to support Romaniello's results, but the uncertainty on these determinations of the metallicity effect from pulsation theory still seems to be rather substantial. In the most recent work on the subject, Wielgórski et al. (2017), using the extremely well-established Cepheid PL relations in the Magellanic Clouds in optical and near-infrared bands combined with the accurate distance determinations to the LMC (Pietrzyński et al. 2013) and SMC (Graczyk et al. 2014) from late-type eclipsing binaries, found a metallicity effect compatible with zero in all bands. As a conclusion, there is still no consensus about the true effect of metallicity on Cepheid absolute magnitudes in different spectral regions. It is especially important to obtain a truly accurate determination of the metallicity effect in the near-infrared bands since these have been used, due to their much lower sensitivity to extinction, in the space-based work on H_0 with the *Hubble* Space Telescope over the last two decades, and will be used in the near future with the *James Webb* Space Telescope.

We present here new and improved measurements of the metallicity effect by direct distance determinations to sizeable samples of Cepheids in the Milky Way, LMC and SMC galaxies, using the infrared surface brightness (IRSB) technique originally introduced by Fouqué & Gieren (1997). This technique was applied to Galactic Cepheids for the first time by Gieren et al. (1997, 1998) demonstrating the great improvement in the accuracy of the Cepheid distances compared to the earlier version of the technique which had used the $(V-R)$ color index as a surface brightness indicator (Gieren et al. 1993). The IRSB technique was later improved by Gieren et al. (2005) and by Storm et al. (2011a), and applied to extra galactic Cepheids (Storm et al. 2004b). In Storm et al. (2004b) we demonstrated that the IRSB technique itself is capable of yielding distances to Cepheids which are independent of their metallicities. In Storm et al. (2011b) we analyzed samples of Cepheids in the Milky Way (MW), in the LMC, and a few in the SMC and found no significant metallicity effect in the K band, and a marginally significant effect of -0.23 ± 0.10 mag dex^{-1} in the optical $V, (V-I)$ Wesenheit index. This result is valid for the metallicity range between solar and -0.35 dex, which is the mean metallicity of classical Cepheids in the LMC (e.g., Luck et al. 1998). However, since the Cepheid populations in the outer part of massive spiral galaxies typically have metallicities comparable to those in the SMC (e.g., Bresolin et al. 2009), it is very important to extend the determination of the metallicity effect down to the -0.73 dex metallicity of SMC Cepheids. A perfect opportunity to do so is a distance determination to a sample of SMC Cepheids using the very same IRSB technique we had used before on MW and LMC Cepheids, and compare the absolute PL relations defined by these distances with those we had previously obtained for the Cepheid samples in the more metal-rich MW and LMC galaxies. We note here that this approach is purely differential and does not depend directly on the true value of the Cepheid absolute magnitude scale. It is thus robust even if the Cepheid absolute magnitude scale might change a bit as more accurate geometric parallaxes to Cepheids become available (e.g., Gaia Collaboration 2017; Riess et al. 2018). We show in the following sections that we now obtain small but significant metallicity effects in the near-infrared and the optical bands, in the sense that the most metal-poor sample of Cepheids (the SMC sample) exhibits PL relations shifted to fainter absolute magnitudes compared to MW and LMC.

2. Data

2.1. Sample

Based on the OGLE survey (Udalski et al. 2008) we selected a sample of 26 Cepheids distributed over the face of the SMC that appeared to be little affected by crowding and that span the range of pulsation periods from 4 to 70 days. In addition to these stars, we also included the five stars HV 822, HV 1328, HV 1333, HV 1335, and HV 1345 analyzed by Storm et al. (2004b) and the star HV 837, which was analysed by Groenewegen (2013). To make efficient use of the near-IR imager we looked for fields which contained several Cepheids. We succeeded in finding seven fields containing more than one Cepheid. In Table 1 the individual fields are listed and in Fig. 1 we show the location of the individual stars as well as the actual fields of the SOFI near-IR imager. It can be seen that about half of the stars are in the central part of the SMC, while the other half samples the outer parts.

While all of the SMC Cepheids in our sample had previous V- and I-band light curves from the OGLE Project, the application of the near-IR surface brightness technique requires full and precise radial curves and K-band light curves. ESO granted us time through a Large Programme, which we have supplemented with additional observations from other facilities. These new data are described and discussed in the following subsections.

2.2. K-band photometric data

The K-band data presented in this paper were collected with the ESO NTT telescope at the La Silla observatory in Chile, equipped with the SOFI near-IR camera (Moorwood et al. 1998). We used the `LARGE_FIELD_IMAGING` setup; the field of view was 4.9×4.9 arcmin, with a scale of 0.288 arcsec pixel^{-1}. A total of 754 data points were collected including the

Table 1. Cepheids in the sample grouped according to field.

ID	RA	Dec	N_n	N_{cal}	Std.dev.	$\sigma(ZP)$
0320	00:39:33.82	−73:44:54.3	25	12	0.015	0.006
1977	00:52:56.82	−71:55:03.3	26	14	0.011	0.004
2533	00:56:20.90	−73:23:13.9	21	10	0.018	0.008
2905	00:58:55.06	−72:33:07.5	31	14	0.015	0.005
3311	01:01:49.49	−72:05:45.4	25	14	0.010	0.004
4017	01:08:11.60	−72:31:18.3	24	13	0.012	0.005
3927	01:07:17.54	−73:13:26.1	24	12	0.020	0.008
4444	01:14:28.07	−72:39:53.6	17	9	0.011	0.005
0958	00:47:10.43	−72:57:37.9	24	14	0.014	0.005
0518	00:43:12.35	−73:19:31.8	22	13	0.013	0.005
0524	00:43:18.77	−73:20:19.8	22	13	0.013	0.005
1686	00:51:26.08	−72:53:18.4	28	17	0.014	0.004
1693	00:51:27.36	−72:51:35.1	28	17	0.014	0.004
1385	00:49:44.60	−73:08:23.1	27	17	0.020	0.006
1410	00:49:55.28	−73:09:16.2	27	17	0.020	0.006
1365	00:49:40.95	−73:14:07.0	24	14	0.021	0.008
1403	00:49:52.88	−73:14:41.0	24	14	0.021	0.008
1680	00:51:24.40	−73:00:17.9	28	15	0.020	0.007
1723	00:51:39.32	−73:01:30.6	28	15	0.020	0.007
1729	00:51:40.67	−73:21:44.3	26	17	0.015	0.005
1750	00:51:49.15	−73:21:55.5	26	17	0.015	0.005
1765	00:51:54.98	−73:22:04.0	26	17	0.015	0.005
1712	00:51:36.22	−73:06:15.1	33	19	0.010	0.003
1717	00:51:38.26	−73:04:43.4	33	19	0.010	0.003
1761	00:51:53.58	−73:06:01.6	33	19	0.010	0.003
1797	00:52:00.35	−73:05:22.3	33	19	0.010	0.003
					mag	mag

Notes. The first group is all the fields containing a single Cepheid. The following groups show the remaining stars and fields. The table gives the OGLE-SMC-CEP identifier, the coordinates (J2000.0), the number of nights (N_n) the Cepheid has been observed, and the number of those nights (N_{cal}) that also had standard star observations. Finally the standard deviation of the photometric zero points from those nights and the resulting estimated zero point uncertainty are given.

data for three additional stars (OGLE-SMC-CEP-1413, -1696, and -1812) for which we do not have radial velocity data. All the data is given in Table 2.

The observations were performed between October 10, 2012, and September 23, 2017. Twenty-six selected Cepheids were grouped in 16 fields, containing from one to four Cepheids in each field. During this period each field was observed between 17 and 33 times. If the conditions were photometric, a set of different UKIRT (Hawarden et al. 2001) standard stars spanning a wide range of colors was observed. It allowed us to calibrate our measurements to the standard system of between 9 and 19 nights for each star depending on the field.

In order to account for frequent sky level variations, the observations were performed with a jittering technique. The number of jittering positions, integration time, and consecutive observations were chosen each night for each field separately to provide the best quality of images. The integration time varied from 3s to 8s in the K band, with one to four consecutive observations, and 21 to 25 jittering positions.

The reduction process of all images followed the approach described in Pietrzyński & Gieren (2002). After basic calibration routines (dark correction, bad pixel correction), sky subtraction was performed with a two-step process implying masking stars with the XDIMSUM IRAF package. Subsequently, the single images were flat-fielded and stacked into the final images.

After the reduction process we performed PSF photometry using DAOPHOT (Stetson 1987) and ALLSTAR (Stetson 1994) routines, following the procedure described in Pietrzyński et al. (2002). The list of star positions was created for each file, based on the best quality images in our sample. This star position list was consequently used to obtain photometry for each field for all nights. In all images around 30 candidate stars for the PSF model were selected, and the PSF model was obtained in an iterative way by subtracting neighboring stars. The aperture corrections were obtained with aperture photometry of 30 previously selected isolated stars, with subtracted neighboring objects. To obtain the light curve, the coordinates of stars on separate images were transformed and cross-matched using DAOMATCH and DAOMASTER (Stetson 1994).

Cepheid differential brightness was calculated by comparison with the selected sample of 26 stars in each field. The random photometric uncertainty on the zero points, $\sigma(ZP)$, is reported in Table 1 for each field. For about half of the light curve points at different phases, the calibrated brightness on the UKIRT standard system was available. We used this to shift the light curve to obtain the light curve on the UKIRT standard system. The Cepheid calibrated brightness dispersion varies for each object from 0.01 and 0.02 mag. The corresponding calibration accuracy of the light curve for each Cepheid is below 0.008 mag.

The SOFI data are originally time stamped with the Modified Julian Date (MJD) which we converted to Julian Date (JD) by adding 2 400 000.5 days.

Our data are on the UKIRT system (Hawarden et al. 2001), but for the IRSB analysis we converted the data to the SAAO system (Carter 1990) to be consistent with the $(V-K)$ surface-brightness relation used in the analysis. We did this using the transformations given by Carpenter (2001).

We supplemented these K-band data with the data from the VMC survey (Cioni et al. 2011; Ripepi et al. 2016) wherever available, except for a few bright stars that show excessive scatter (OGLE-SMC-CEP-1797, -1977, -3311, -3927), likely caused by saturation issues for the VMC data. In this way all of the stars have well-sampled light curves in the K band with between 20 and 40 data points. The VMC data is on the VISTA system so we convert it first to the 2MASS system as described in Ripepi et al. (2016) and then to the SAAO system as described in Carpenter (2001). We then applied small zero point shifts to the VMC magnitudes for each star to ensure the best agreement between the two data sets. One star (OGLE-SMC-CEP-1365) showed a significant offset of +0.18 mag. For the remaining stars the mean offset was only −0.01 mag with a standard deviation of 0.01 mag which gives us confidence that the photometric zero point is very well established. Our K-band photometric data is presented in Table 2 and the light curves for stars can be found in Figs. A.1–A.26. Where appropriate the VMC data with the proper zero point offsets applied have been overplotted in these figures.

The VMC survey (Ripepi et al. 2016) also provides mean J-band magnitudes based on a few (≈6) phase points which have been fitted with a template light curve. These mean magnitudes have been adopted here to derive the PL-relation in the J band and for the Wesenheit index in $(J-K)$. Ripepi et al. (2016) estimate that for 93% of the stars the error on the thus derived J-band mean magnitude is below 0.02 mag.

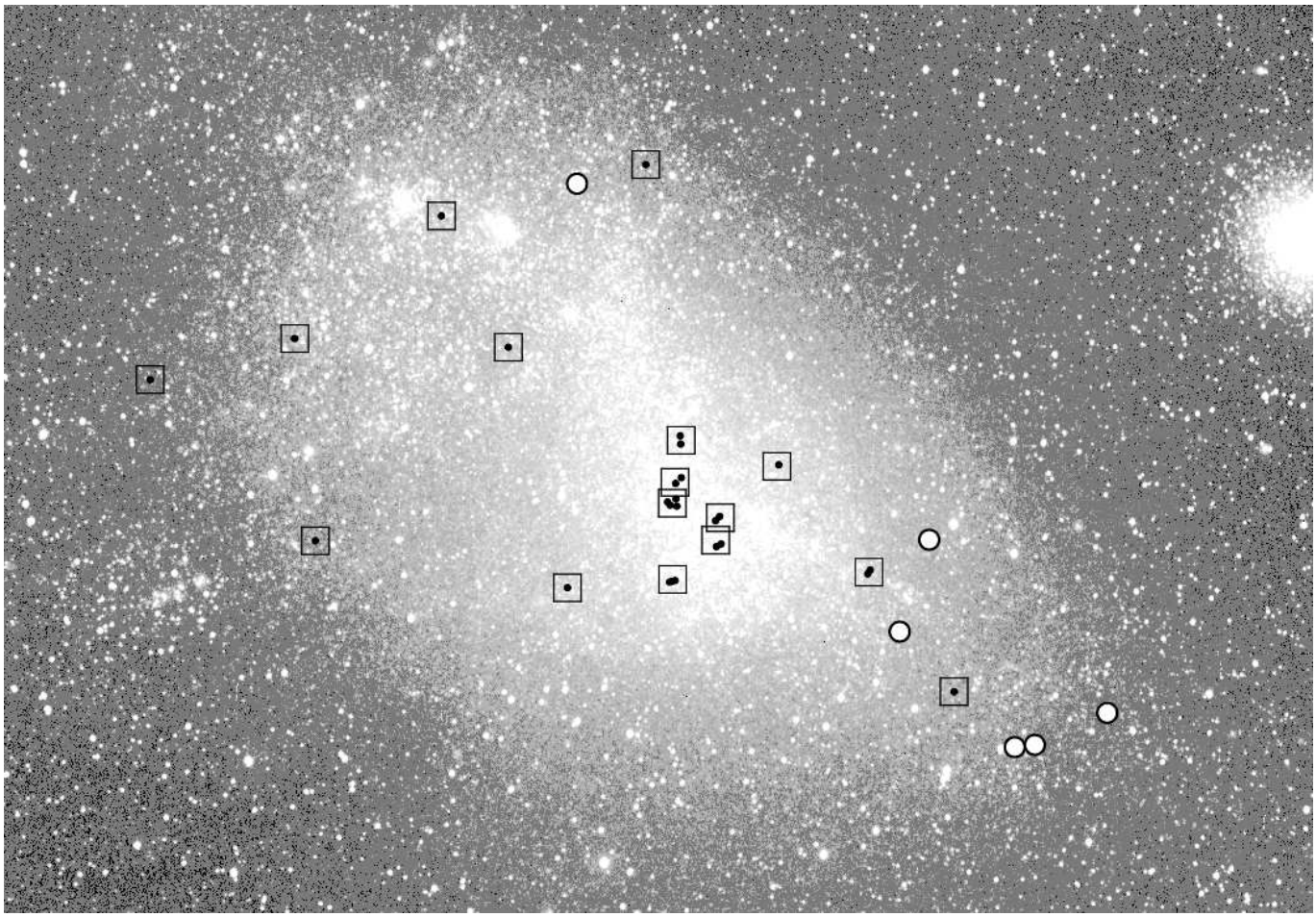

Fig. 1. Location of the Cepheids in the SMC: black dots for the new stars and filled circles for the six stars studied previously. The boxes are indicative of the field size of the SOFI near-IR imager. The underlying image was obtained by ASAS and is from Udalski et al. (2008).

Table 2. *K*-band data in the UKIRT system as observed with SOFI.

Identifier	JD	*K*	σ
OGLE-SMC-CEP-0320	2456211.57648	12.505	0.002
OGLE-SMC-CEP-0320	2456211.78426	12.514	0.004
OGLE-SMC-CEP-0320	2456212.55166	12.509	0.004
OGLE-SMC-CEP-0320	2456213.67309	12.507	0.002
OGLE-SMC-CEP-0320	2456214.78703	12.517	0.002
OGLE-SMC-CEP-0320	2456233.51368	12.532	0.003
OGLE-SMC-CEP-0320	2456234.53185	12.551	0.003
OGLE-SMC-CEP-0320	2456235.51983	12.577	0.004
OGLE-SMC-CEP-0320	2456247.67128	12.515	0.004
OGLE-SMC-CEP-0320	2456529.76325	12.536	0.002
...			
	days	mag	mag

Notes. The photometry is given together with the Julian Date (JD), and the estimated measurement error. The full table is available at CDS.

2.3. Optical light curves

V- and *I*-band light curves were obtained from the OGLE-III and OGLE-IV surveys (Udalski et al. 2008, 2015; Soszyński et al. 2008, 2015). We adopted in all cases the photometric zero point defined by the OGLE-III survey and shifted the OGLE-IV data onto the same system. Plots of the *V*-band light curves can be found in Appendix A.

Table 3. Cross-identification of the Harvard variables from earlier studies and the OGLE data base.

OGLE identifier	HV identifier
OGLE-SMC-CEP-0431	HV 822
OGLE-SMC-CEP-2470	HV 837
OGLE-SMC-CEP-0152	HV 1328
OGLE-SMC-CEP-0230	HV 1333
OGLE-SMC-CEP-0246	HV 1335
OGLE-SMC-CEP-0368	HV 1345

2.4. Harvard variables from earlier studies

For the five stars which were studied earlier in Storm et al. (2004b) we used the data from Storm et al. (2004a) and Welch et al. (1987), and for HV 837 we used the data from Udalski et al. (2008) (*V* band) and Laney & Stobie (1986; *K* band). The cross-identification with the OGLE catalogue is given in Table 3. For all these stars the data were supplemented with the VMC (Ripepi et al. 2016) and OGLE (Udalski et al. 2015; Soszyński et al. 2015) data. The star HV1345 showed a phase shift corresponding to 0.3 days between the old data and the newer data, we shifted the old data accordingly. For the *V*-band data we kept the old photometric zero points as they were in good agreement for three of the stars, but for the two stars HV 1333 and HV 1345 we shifted the OGLE-IV data by

−0.04 and −0.05 mag, respectively. Where necessary we shifted the old K-band data to the VMC system, appropriately shifted to the SAAO system as described in the previous section. In the case of HV 1345 the shift was +0.11 mag, while for the remaining stars the shifts were on average −0.01 mag with a standard deviation of 0.03 mag. Finally, we shifted these K-band magnitudes by the mean VMC offset of −0.01 mag to be consistent with the adopted SOFI photometric zero point.

2.5. Reddening

For the reddening law we proceeded exactly as in Storm et al. (2011a), but note that assuming a universal reddening law for the three galaxies is not strictly correct (e.g., Alonso-García et al. 2017). We adopted the reddening law by Cardelli et al. (1989) and used a ratio of total to selective absorption of $R_V = 3.23$, $R_I = 1.96$, $R_J = 0.292R_V$, and $R_K = 0.119R_V$ following the discussion in Fouqué et al. (2007). The reddening of our stars was based on the photometric $E(V-I)$ reddening maps derived by Haschke et al. (2011) based on OGLE photometry (Udalski et al. 2008; Soszyński et al. 2008) of red clump stars. These reddenings are not based on intrinsic Cepheid colors so they are independent of the metallicities of the Cepheids, which is relevant in the present study as we are looking for metallicity effects on the PL relations. We determined $E(B-V)$ from $E(B-V) = E(V-I)/(R_V - R_I) = E(V-I)/1.27$. To verify that we were on the same reddening system as adopted in our previous work, we compared the reddening values for the 26 LMC Cepheids in Storm et al. (2011b) which are within the area of the Haschke et al. reddening map. The two reddening systems show excellent agreement with an average difference of 0.006 ± 0.007 mag with a standard deviation of 0.035 mag. Inno et al. (2016) using multiband photometry ranging from the optical (VI) over the near-IR (JHK_s) to the mid-IR Wise $w1$ band for a large sample of LMC Cepheids have determined individual reddenings for these Cepheids based on the multiband PL relations. They also find that their values are in reasonable agreement with the maps from Haschke et al. (2011) even if they are derived in an entirely independent way. Inno et al. (2016) report an even better agreement with the reddenings for eclipsing binary stars as reported by Pietrzyński et al. (2013) based on the work of Graczyk et al. (2012). They used the equivalent width of the NaI D1 line in spectra of eclipsing binary stars to determine the reddening directly, as well as employing a calibration of the spectroscopically determined effective temperatures with the photometric $(V-I)$ and $(V-K)$ colors to infer the reddening. This work has been further developed by Graczyk et al. (2014, 2018) and we adopted the reddening values from latter work and determined the unreddened $(V-I)_0$ color for red clump stars around these eclipsing binaries. This color was then used to determine the reddening for red clump stars in the immediate neighborhood of our Cepheids. We found a shift with respect to the Haschke et al. (2011) values of +0.05 ± 0.01 mag and +0.04 ± 0.01 mag, respectively, for the SMC and LMC samples.

Similarly, recent work by Turner (2016) employing space reddenings suggests that the reddenings adopted for the galactic sample by Storm et al. (2011b), which we use here, should be transformed by the linear relation

$$E(B-V)_{\rm Turner} = 0.020_{\pm 0.006} + 1.067_{\pm 0.019} E(B-V)_{\rm Storm11}. \quad (1)$$

The galactic sample has a mean reddening of about $E(B-V) = 0.5$ mag which would lead to an overall increase in the reddening of about +0.05 mag so very similar to the shifts suggested for the Magellanic Cloud samples. It thus seems that the reddenings for all three samples should be shifted by about the same amount, and consequently the relative luminosities, our main concern in the present work, would not change by much. We thus prefer to continue the use of the original reddening scales adopted in Storm et al. (2011b), but include the uncertainty on the reddening estimate in the final error estimate. Considering the systematic offsets between recent works we estimate the uncertainty to be $\sigma_{\rm sys}(E(B-V)) = 0.05$ mag.

The adopted reddening values from Haschke et al. (2011) are given in Table 5. We can see that the reddenings are in general very small (≈0.05 mag) so the exact choice of reddening law is not critical for the SMC stars themselves.

2.6. Radial velocity data

During the five years between October 2012 and October 2017 we obtained a total of 714 radial velocity observations of our sample of 26 SMC Cepheids, using three different high-resolution spectrographs: HARPS (Mayor et al. 2003) at the 3.6m telescope at ESO-La Silla; MIKE (Bernstein et al. 2003) attached to the 6.5m Clay telescope at Las Campanas Observatory; and UVES (Dekker et al. 2000) mounted at the ESO-VLT at the Paranal site of the European Southern Observatory. Great care was taken to schedule the observations in a way so as to assure an optimum phase coverage of the radial velocity curves of the Cepheids with the help of the observation planning software written by one of us (BP): 65% of the data were obtained with HARPS, 29% with MIKE, and 6% with UVES. We adjusted the integration times in order to achieve signal-to-noise ratio values in the range 3–8 for the Cepheids, which is high enough to measure very accurate radial velocities according to our previous extensive experience with the spectrographs used in this study. For the shortest-period and faintest Cepheids we set a limit of 1800 s in the integration times to keep them below 1% of their periods. The HARPS spectra were reduced using the on-site pipeline; MIKE data were reduced with software developed by Dan Kelson (Kelson 2003), and the UVES spectra were reduced with a publicly available ESO pipeline (Freudling et al. 2013).

The radial velocities were measured with the RaveSpan software (Pilecki et al. 2017). This code uses the Broadening Function technique originally introduced by Rucinski (1992, 1999) and a set of synthetic spectra from Coelho et al. (2005) as radial velocity reference templates. For consistency, all spectra were processed in a similar manner, being properly continuum-normalized and analyzed in the same wavelength range within 4125–6800 Å which contains numerous metallic lines. The individual velocities were typically accurate to 250 m s^{-1}.

In the Figs. A.1–A.26 we show the radial velocity curves for Cepheids. The full set of individual radial velocity data is given in Table 4. A significant number of the stars (seven) showed velocity variations indicative of orbital motion. The amplitudes are too large to be caused by amplitude variations as described by e.g. (Anderson 2016) and the smooth variation in the long-term trends also suggests orbital motion. As we did not have enough data to determine a proper binary orbit solution we instead attempted to simply shift the data from different epochs to take out the putative orbital motion. We appealed to continuity arguments and tried to fix the offset for a given epoch by requiring data points at the same phase, but for different epochs to give approximately the same radial velocity. We thus assumed that the variation in the orbital motion is small for a certain period of time, typically hundreds of days, and thus that the orbital period is much longer than the pulsational period. In Appendix B we present the detailed analysis for the individual stars. The stars

Table 4. Radial velocity measurements for the stars are tabulated together with the HJD of the measurement, the estimated error, and the instrument used.

Identifier	HJD	Radial velocity	σ	Instrument
OGLE-SMC-CEP-0320	2456211.81673	160.26	0.03	HARPS
OGLE-SMC-CEP-0320	2456213.72001	164.27	0.06	HARPS
OGLE-SMC-CEP-0320	2456214.79017	166.60	0.07	HARPS
OGLE-SMC-CEP-0320	2456240.53387	164.64	0.20	HARPS
OGLE-SMC-CEP-0320	2456241.52979	161.74	0.03	HARPS
OGLE-SMC-CEP-0320	2456529.84546	160.37	0.04	HARPS
OGLE-SMC-CEP-0320	2456579.62039	170.02	0.05	HARPS
OGLE-SMC-CEP-0320	2456605.55640	159.00	0.03	HARPS
OGLE-SMC-CEP-0320	2456879.84336	169.07	0.03	HARPS
OGLE-SMC-CEP-0320	2456908.72710	159.38	0.04	HARPS
...				
	days	km s^{-1}	km s^{-1}	

Notes. The full table is available at CDS.

in question are OGLE-SMC-CEP-1680, -1686, -1693, -1729, -1977, -2905, and HV 837. In the case of OGLE-SMC-CEP-1686 the radial velocity amplitude is quite small and it was difficult to find consistent velocity offsets, so we prefered to leave the data unchanged for this star. In the case of OGLE-SMC-CEP-1693 the offsets seem to be large but we did not manage to find sensible offsets and this star had to be disregarded in the further analysis. We nevertheless include the observed radial velocities in Table 4.

For the stars that were analyzed previously by Storm et al. (2004b), we used the radial velocities from Storm et al. (2004a); for HV 837, analyzed by Groenewegen (2013), we used the radial velocity measurements from Imbert et al. (1989).

3. Analysis

We apply the near-IR surface-brightness (IRSB) method to the data following exactly the same procedures and calibrations as adopted and described by Storm et al. (2011a). In this way we ensure that we can perform a purely differential comparison with the results for the Milky Way and LMC samples from that study.

We note that Mérand et al. (2015) have recently developed a new implementation of the method in a code named SPIPS, which can utilize more observational data (more photometric bands, interferometric data) and has a more complex data processing system. As we do not have additional data for the SMC Cepheids and want to make a purely differential comparison with the LMC and Milky Way samples, we proceed with the IRSB method as calibrated in Storm et al. (2011a).

The IRSB method is a Baade-Wesselink-type of technique which utilizes the stellar radial pulsation to determine the distance and radius of the star. This is achieved by geometrically matching the angular diameter variation of the star with the absolute radius variation,

$$\theta(\phi) = 2R(\phi)/d = 2(R_0 + \Delta R(\phi))/d, \quad (2)$$

where θ is the angular diameter, ϕ is the pulsation phase, d is the distance, R is the stellar radius, R_0 the average radius, and $\Delta R(\phi)$ the radius difference with respect to the average radius.

The angular diameter is determined from the surface-brightness, F_V, through the relation

$$F_V(\phi) = 4.2207 - 0.1V_0(\phi) - 0.5\log\theta(\phi), \quad (3)$$

where V_0 is the dereddened V-band magnitude at a given phase.

As shown first by Welch (1994), F_V is a nearly linear function of the $(V-K)_0$ color index. This is the near-IR version of the Barnes-Evans method (Barnes & Evans 1976). Welch (1994) also pointed out the significantly reduced scatter in the relation compared to purely optical color indices while maintaining the low sensitivity to reddening errors. An error of 0.06 mag in $E(B-V)$ only causes an error of 0.03 mag in the derived distance. The calibration was later refined by Fouqué & Gieren (1997), Kervella et al. (2004), and others based on more modern interferometrically determined stellar radii and in the case of Kervella et al. (2004) also using interferometrically determined angular diameters of Cepheids. Several groups (e.g., Boyajian et al. 2013; Challouf et al. 2014; Graczyk et al. 2017) have presented much expanded empirical calibrations for non-variable stars that will potentially improve the method. The $(V-K)_0$ surface-brightness relation has been shown to be almost metallicity independent (Storm et al. 2004b; Thompson et al. 2001). Thompson et al. (2001) find only a 1% effect going from [Fe/H] = 0.0 to −2.0. In the present work we need to be consistent with Storm et al. (2011a,b), and we thus adopt the calibration of the surface-brightness as a function of the $(V-K)_0$ color index from Kervella et al. (2004):

$$F_V = -0.1336(V-K)_0 + 3.9530. \quad (4)$$

The other observable in Eq. (2) is the radial velocity, $V_r(\phi)$, at a given phase. This can be used to determine the radius variation by integrating the pulsational velocity:

$$\Delta R(\phi) = \int -p[V_r(\phi) - V_\gamma]d\phi \quad (5)$$

To compute the pulsational velocity it is necessary to subtract the systemic velocity, V_γ, and multiply by the so-called projection factor, p, which takes into account that the observed radial velocity refers to the integrated light from the observed hemisphere of the star. The factor p is mostly a geometric effect, but is also affected by limb darkening and velocity gradients in the dynamical atmosphere of the pulsating star (see, e.g., Nardetto et al. 2017; and references therein). Storm et al. (2011a) calibrated the p-factor applicable for the IRSB method and we adopt here the exact same relation:

$$p = 1.55 - 0.186\log(P). \quad (6)$$

Other recent empirical efforts to determine the projection factor for Cepheids, and its dependence on pulsation period, agree with our findings (e.g., Pilecki et al. 2018) and have produced a milder dependence (e.g., Gallenne et al. 2017) or even values consistent with a zero period dependence of the p-factor (Kervella et al. 2017). However, these studies show a large scatter among the projection factors of individual Cepheids, hinting at large systematic uncertainties on the individual determinations (Kervella et al. 2017) and/or a possible intrinsic dispersion of the p-factors of Cepheids of similar periods. As shown by the hydrodynamical Cepheid models by Nardetto et al. (2011), the p-factor shows no significant dependence on metallicity. This means that the differential metallicity effect we determine here is largely independent on the exact choice of the p-factor relation.

In Figs. 2–3 the fits for two typical stars with different pulsation periods are shown. In the case of the star OGLE-SMC-CEP-1385 (Fig. 3) with a period of about 16 days a typical bump in the photometric angular diameter curve can be seen. As in the previous work we disregard the phase interval from 0.8 to 1.0 when performing the fits to avoid this region where shock waves are known to be present in the stellar atmospheres, thus possibly affecting the surface brightness-color relation.

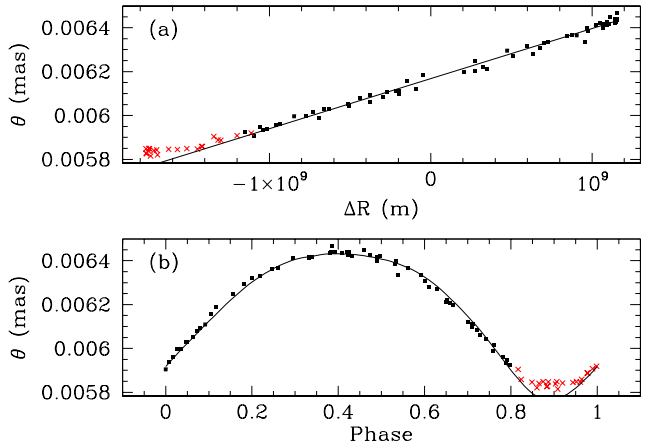

Fig. 2. Example of the actual fit of the angular diameters from photometry and the radius variation from the radial velocity curve (*panel a*) for the 5.6-day period star OGLE-SMC-CEP-1765. In *panel b* the corresponding match of the angular diameters curve from the photometry (points) and from the radial velocity curve is plotted. The points marked with red crosses have not been considered in the fit.

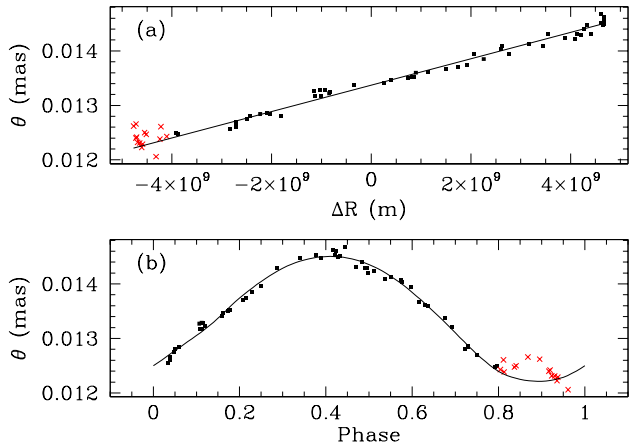

Fig. 3. Example of the actual fit of the angular diameters from photometry and the radius variation from the radial velocity curve (*panel a*) for the 16-day period star OGLE-SMC-CEP-1385. In *panel b* the corresponding match of the angular diameters curve from the photometry (points) and from the radial velocity curve is plotted. The points marked with red crosses have not been considered in the fit.

4. Metallicities

As was the case for Storm et al. (2011b), we do not have individual metallicities for our LMC and SMC Cepheids. We proceed as in that analysis and we adopt mean metallicities for each of the three samples of Milky Way, LMC, and SMC Cepheids, thus treating the three samples in the same way.

As we are looking for differential effects it is particularly important that the values are on the same system. Romaniello et al. (2008) made a detailed study of Cepheids in all three galaxies. The Milky Way sample consists of 32 stars, the LMC sample of 22 Cepheids and the SMC sample of 14 Cepheids. The mean metallicities are 0.00 ± 0.02, −0.34 ± 0.03, −0.75 ± 0.02 with dispersions of 0.12, 0.15, and 0.08 dex, respectively. For 25 of our Milky Way stars Romaniello et al. (2008) reports metallicities and they show an average value of −0.01 ± 0.02 dex.

For the Milky Way sample Groenewegen (2013) has compiled a list of individual metallicities based on the measurements by Luck & Lambert (2011), Luck et al. (2011), Fry & Carney (1997), Andrievsky et al. (2003), and Romaniello et al. (2008). We found metallicities for 64 of our MW Cepheids in this list, and after applying the offsets between samples as determined in that paper we find an average value of [Fe/H] = +0.07 ± 0.01. This value is slightly different from that found by Romaniello et al. (2008), but comparable to the offsets between works found by Romaniello et al. (2008) and Groenewegen (2013). If we look for the 25 stars also present in the study of Romaniello et al. (2008), we find a mean value of +0.07 ± 0.03, in good agreement with the value from the full sample, so this smaller sample is still very representative of our full MW sample.

Recently Lemasle et al. (2017) have measured metallicities for four SMC Cepheids and for six Cepheids in the LMC young blue cluster NGC 1866. These values are in good agreement with the values from Romaniello et al. (2008) with a slight offset of +0.03 dex leading to mean abundances of the combined samples of −0.73 ± 0.02 and −0.33 ± 0.03 dex, respectively. Molinaro et al. (2012) also measured metallicities for three Cepheids in NGC1866 and found a mean value of −0.40 ± 0.04 in good agreement with the value of −0.36 ± 0.03 from Lemasle et al. (2017). Lemasle et al. (2013) has similarly determined abundances for Milky Way Cepheids and for 12 stars in common with our sample the average metallicity is −0.07 ± 0.04 dex. The metallicity range in this case is slightly narrower than was the case when we employed the Romaniello et al. (2008) metallicities. Genovali et al. (2014) has measured metallicities for ten of our stars and they on the other hand find a mean metallicity of +0.05 ± 0.03 dex. So these four sources for the metallicity for Milky Way Cepheids range between −0.07 and +0.07. We prefer to use the Romaniello et al. (2008) value of 0.00 as it is obtained in a self-consistent way with the LMC and SMC metallicities, although we add in quadrature a systematic error contribution on the metallicities of 0.05 to reflect a possible uncertainty in the metallicity scale. To summarize, we adopt for the MW, LMC, and SMC samples the values +0.00 ± 0.05, −0.34 ± 0.06, and −0.75 ± 0.05 dex.

5. Results

In Table 5 the derived distance moduli and associated fitting errors are given for all the stars in the sample. We emphasize that these are fitting errors only. Barnes et al. (2005) compared these error estimates with error estimates from a full Bayesian analysis of the data and found that, on average, these errors are underestimated by about a factor of 3.4. In particular the fitting errors can sometimes be very small as the data line up almost perfectly on a straight line. Such small errors can significantly skew weighted fits, so we prefer here to use unweighted fits for our PL relations. The table is sorted according to pulsation period, and it includes the resulting absolute magnitudes and Wesenheit indices, adopted reddenings, and the usually very small phase shifts we needed to apply to obtain a best match between angular diameter and linear displacement curves.

We have plotted the distance moduli of the stars versus $\log P$ in Fig. 4. Linear regression gives a marginally significant slope of −0.15 ± 0.13 still compatible with no period dependence. We have computed the average of the distance moduli to the Cepheids in the sample and find $(m - M)_0 = 18.86 \pm 0.04$ mag. Discarding the seven possible binaries in our sample, the mean distance modulus changes by just 0.01 mag, which is not significant and supports our procedure for correcting the observed radial velocities of these stars for binary motion (see Appendix B). We can also compute the difference in the distance

Table 5. Distances and absolute magnitudes of the SMC Cepheids.

(1) ID	(2) log(P)	(3) d	(4) $\sigma_{\mathrm{FIT},d}$	(5) $(m-M)_0$	(6) $\sigma_{\mathrm{FIT},(m-M)}$	(7) M_V	(8) M_I	(9) M_J	(10) M_K	(11) W_{VI}	(12) W_{JK}	(13) $E(B-V)$	(14) $\Delta\phi$
OGLE-SMC-CEP-1761	0.595415	63.6	1.2	19.02	0.04	−2.79	−3.49	−4.03	−4.36	−4.56	−4.58	0.024	0.005
OGLE-SMC-CEP-1729	0.631889	62.7	0.6	18.99	0.02	−2.71	−3.46	−4.10	−4.37	−4.61	−4.55	0.024	0.025
OGLE-SMC-CEP-1680	0.689176	63.7	1.2	19.02	0.04	−3.14	−3.83	−4.33	−4.71	−4.91	−4.98	0.031	0.000
OGLE-SMC-CEP-1765	0.750044	58.6	0.6	18.84	0.02	−2.87	−3.62	−4.15	−4.55	−4.78	−4.83	0.024	0.010
OGLE-SMC-CEP-1717	0.823504	61.3	0.8	18.94	0.03	−3.13	−3.92	−4.48	−4.90	−5.14	−5.19	0.024	0.005
OGLE-SMC-CEP-1410	0.963223	56.4	0.9	18.75	0.04	−3.71	−4.48	−4.97	−5.44	−5.67	−5.76	0.055	0.005
OGLE-SMC-CEP-1712	1.006814	62.7	0.5	18.99	0.02	−3.51	−4.43	−5.07	−5.53	−5.85	−5.84	0.024	0.020
OGLE-SMC-CEP-0524	1.022321	62.5	0.8	18.98	0.03	−3.74	−4.54	−5.08	−5.53	−5.78	−5.83	0.047	0.020
OGLE-SMC-CEP-2533	1.084483	50.5	1.0	18.52	0.04	−3.97	−4.66	−5.16	−5.51	−5.73	−5.75	0.024	0.025
HV 1345	1.129670	55.7	1.4	18.73	0.05	−4.08	−4.80	−5.32	−5.79	−5.90	−6.10	0.031	−0.015
HV 1335	1.157800	53.1	0.8	18.62	0.03	−3.94	−4.71	−5.22	−5.67	−5.89	−5.98	0.024	−0.020
OGLE-SMC-CEP-1365	1.194727	61.9	1.8	18.96	0.06	−4.56	−5.34	−6.05	−6.33	−6.55	−6.51	0.055	0.035
OGLE-SMC-CEP-0518	1.197888	63.4	0.8	19.01	0.03	−4.00	−4.95	−5.60	−6.08	−6.42	−6.41	0.055	0.010
OGLE-SMC-CEP-1385	1.199259	55.3	1.0	18.71	0.04	−4.12	−4.96	−5.57	−6.03	−6.25	−6.34	0.055	0.020
HV 1328	1.199692	47.7	1.1	18.39	0.05	−4.32	−5.02	−5.45	−5.83	−6.11	−6.09	0.016	0.015
HV 1333	1.212084	71.0	1.4	19.25	0.04	−4.65	−5.46	−6.02	−6.50	−6.71	−6.82	0.024	−0.020
OGLE-SMC-CEP-1723	1.215794	68.2	0.8	19.17	0.03	−4.25	−5.22	−5.89	−6.36	−6.70	−6.68	0.024	0.010
HV 822	1.223807	65.4	1.9	19.08	0.06	−4.69	−5.50	−6.01	−6.48	−6.76	−6.80	0.039	−0.020
OGLE-SMC-CEP-0320	1.253893	54.1	0.4	18.66	0.02	−4.59	−5.28	−5.75	−6.10	−6.34	−6.35	0.031	0.015
OGLE-SMC-CEP-1750	1.310784	67.6	1.2	19.15	0.04	−4.62	−5.56	−6.18	−6.71	−7.01	−7.08	0.024	−0.005
OGLE-SMC-CEP-0958	1.379643	62.9	0.5	18.99	0.02	−4.81	−5.67	−6.29	−6.82	−7.01	−7.17	0.031	0.005
OGLE-SMC-CEP-1403	1.459128	54.2	0.4	18.67	0.02	−4.49	−5.44	−6.10	−6.66	−6.91	−7.05	0.055	0.005
OGLE-SMC-CEP-3927	1.517905	54.0	0.6	18.66	0.03	−5.08	−5.85	−6.50	−7.00	−7.03	−7.34	0.055	0.020
OGLE-SMC-CEP-4017	1.527325	54.0	1.5	18.66	0.06	−5.04	−5.96	−6.41	−7.02	−7.38	−7.45	0.039	0.040
OGLE-SMC-CEP-1686	1.540177	64.6	1.2	19.05	0.04	−5.70	−6.53	−7.02	−7.53	−7.80	−7.88	0.063	0.030
OGLE-SMC-CEP-2905	1.580231	61.6	0.8	18.95	0.03	−5.21	−6.22	−6.75	−7.37	−7.77	−7.80	0.079	0.035
OGLE-SMC-CEP-1797	1.615447	54.4	0.7	18.68	0.03	−4.97	−6.00	−6.55	−7.27	−7.58	−7.76	0.024	0.025
OGLE-SMC-CEP-4444	1.621557	75.5	1.4	19.39	0.04	−6.52	−7.33	−7.90	−8.30	−8.57	−8.57	0.031	0.095
HV 837	1.630904	59.6	0.9	18.88	0.03	−5.72	−6.64	−7.11	−7.71	−8.07	−8.12	0.024	0.035
OGLE-SMC-CEP-3311	1.696679	49.1	0.8	18.45	0.04	−5.31	−6.34	−6.56	−7.54	−7.93	−8.22	0.024	−0.045
OGLE-SMC-CEP-1977	1.838831	50.2	1.0	18.50	0.04	−5.69	−6.72	−7.16	−7.91	−8.32	−8.42	0.031	−0.010
	P in days	kpc	kpc	mag	mag	mag	mag	mag	mag	mag	mag	mag	

Notes. For each star we give the identifier and the logarithm of the period in days, log(P). The resulting distances and their associated formal fitting errors are given in Cols. (3) and (4); in Cols. (5) and (6) the distance modulus and formal error are given; Cols. (7)–(12) list the resulting absolute magnitudes; Col. (13) gives the adopted reddening based on Haschke et al. (2011); Col. (14) gives the phase shift adopted in the IRSB fitting.

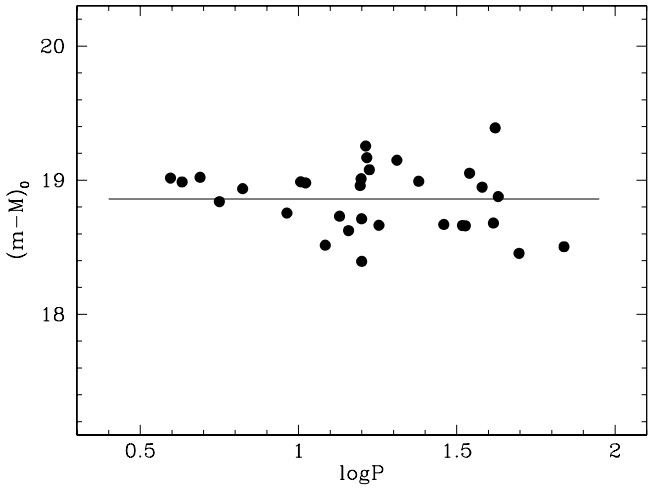

Fig. 4. Derived distance modulus as a function of log P for all the SMC stars. The horizontal line indicates the average value.

Table 6. Period-luminosity relation in the SMC for the various bands in the form $M = \alpha(\log P - 1.0) + \beta$.

Band	α	$\sigma(\alpha)$	β	$\sigma(\beta)$	Std.dev.
M_K	−3.179	0.141	−5.509	0.056	0.24
M_J	−2.856	0.169	−5.098	0.067	0.29
W_{JK}	−3.401	0.133	−5.791	0.053	0.23
M_V	−2.705	0.177	−3.751	0.070	0.30
M_I	−2.934	0.156	−4.536	0.062	0.27
W_{VI}	−3.287	0.148	−5.746	0.059	0.25
			mag	mag	mag

modulus between the LMC ($(m - M)_0 = 18.46 \pm 0.04$ mag; Storm et al. 2011b) and the SMC, and we find $\Delta(m - M)_0 = 0.40 \pm 0.06$ mag.

On the basis of the data in Table 5 we determined the PL relation by linear regression for each band. These relations in the form $M = \alpha(\log P - 1.0) + \beta$ are listed in Table 6. In Figs. 5 and 6 we plot the data in the K band and the reddening insensitive Wesenheit $V, (V - I)$ index, $W_{VI} = V - R_{Wvi}(V - I) - (m - M)_0$, as adopted in Storm et al. (2011a), where $R_{Wvi} = R_V/(R_V - R_I) = 2.54$ with the total-to-selective absorption ratios from Sect. 2.5. We similarly compute the near-IR Wesenheit index $W_{JK} = K - R_{Wjk}(J - K) - (m - M)_0$, where $R_{Wjk} = R_K/(R_J - R_K) = 0.69$. The relations are very well defined and from Table 6 we see that the standard deviation around the best fit is about 0.24 mag for the reddening independent relations (K, W_{VI}, W_{JK}), in very good agreement with the values found by Storm et al. (2011a) for the LMC and MW samples.

As we intended to compare the slopes and zero points for the three different samples, we also determined the relations in the slightly different form of $M = \alpha(\log P - 1.18) + \beta$, where

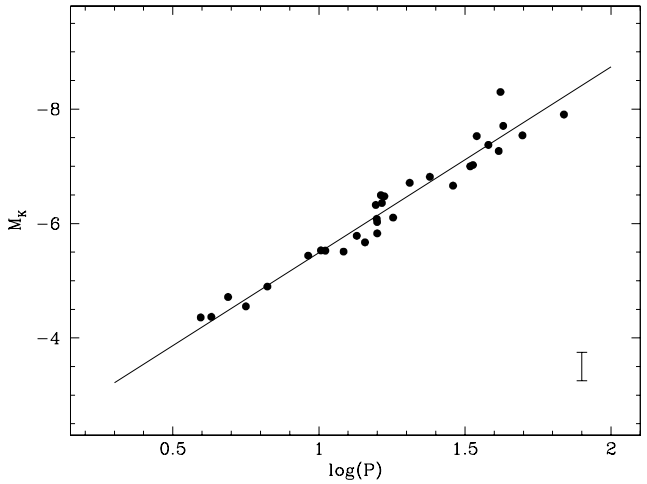

Fig. 5. Period-luminosity relation in the K band for the SMC Cepheids. The line represents the LMC slope as determined by Macri et al. (2015) shifted to match the SMC. A typical error bar is shown in the lower right.

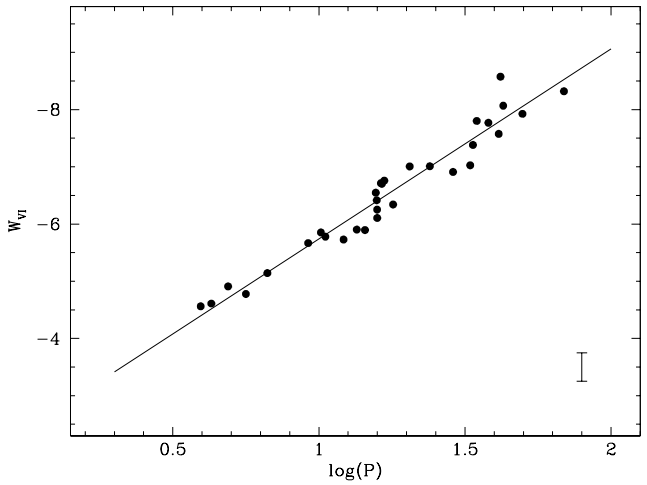

Fig. 6. Period-luminosity relation in the $V,(V-I)$ Wesenheits index for the SMC Cepheids. The line represents the slope as determined by Storm et al. (2011a) for their combined sample, shifted to match the SMC. A typical error bar is shown in the lower right.

log $P = 1.18$ is close to the mid-point of the period range under investigation. In this way the zero point errors are minimized and they are the least correlated with errors in the derived slopes. These relations can be found in Table 7 together with the relations which we have redetermined for the Milky Way and LMC samples from Storm et al. (2011a). From the table it is clear that the slopes of the PL relations in the three different galaxies are in excellent agreement which justifies the assumption of a common, metallicity-independent slope of the PL relation is each band. In Figs. 7 and 8 we have overplotted the data from the three samples in the K band and the Wesenheit $V,(V-I)$ index. It can be seen that the slopes of the different samples appear very similar, but also that there are small shifts of the zero points.

To determine the zero point offsets between the three samples we adopted a slope for the given band and fit the three samples individually. We thus obtained three different zero point values which we list as β in Table 8. We adopted the LMC zero point as the reference and subtracted it from the SMC and MW zero points, respectively, to derive ΔM. In the V

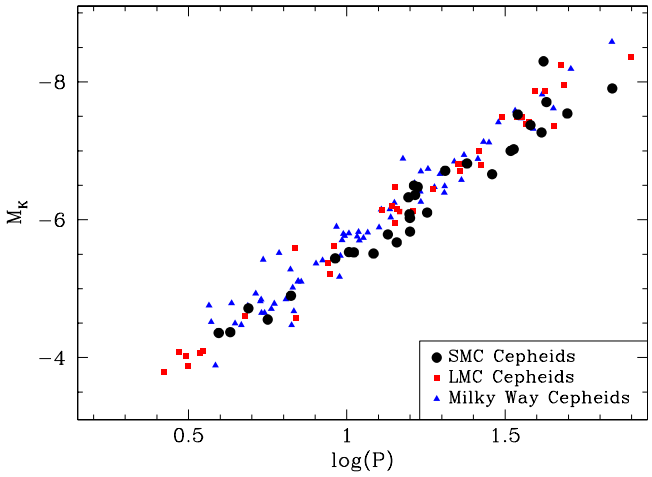

Fig. 7. K-band PL relation for the SMC stars (black) overplotted on the Milky Way (blue triangles) and LMC (red squares) samples.

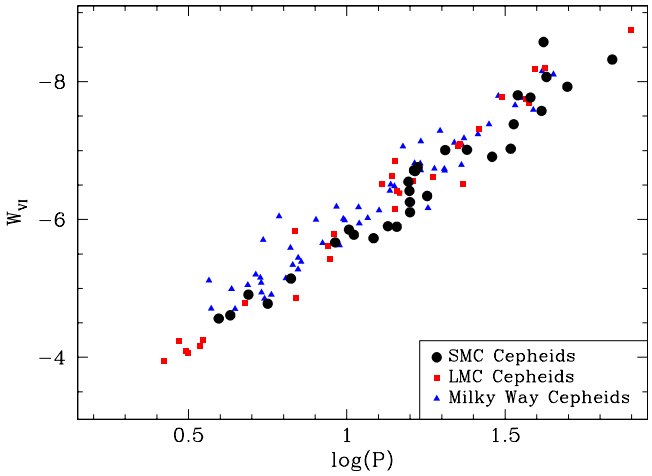

Fig. 8. Wesenheit $V,(V-I)$ index PL relation for the SMC stars (black) overplotted on the Milky Way (blue triangles) and LMC (red squares) samples.

Table 7. Period-luminosity relations for the three different samples and for each band the form $M = \alpha(\log P - 1.18) + \beta$.

Band	Galaxy	α	$\sigma(\alpha)$	β	$\sigma(\beta)$	Std.dev.
M_K	SMC	−3.179	0.141	−6.081	0.046	0.24
M_K	LMC	−3.282	0.087	−6.225	0.036	0.21
M_K	MW	−3.258	0.092	−6.268	0.030	0.23
M_J	SMC	−2.856	0.169	−5.612	0.055	0.29
M_J	LMC	−3.220	0.090	−5.750	0.037	0.21
M_J	MW	−3.114	0.092	−5.802	0.030	0.23
W_{JK}	SMC	−3.401	0.133	−6.404	0.043	0.23
W_{JK}	LMC	−3.324	0.089	−6.552	0.036	0.21
W_{JK}	MW	−3.357	0.097	−6.589	0.032	0.24
M_V	SMC	−2.705	0.177	−4.238	0.057	0.30
M_V	LMC	−2.775	0.111	−4.499	0.045	0.26
M_V	MW	−2.615	0.100	−4.457	0.033	0.25
M_I	SMC	−2.934	0.156	−5.064	0.051	0.27
M_I	LMC	−3.021	0.101	−5.280	0.041	0.21
M_I	MW	−2.664	0.098	−5.293	0.031	0.21
W_{VI}	SMC	−3.287	0.148	−6.338	0.048	0.25
W_{VI}	LMC	−3.411	0.112	−6.484	0.046	0.24
W_{VI}	MW	−3.084	0.117	−6.562	0.037	0.25
				mag	mag	mag

Table 8. Period-luminosity relation with fixed slopes for the various bands in the form $M = \alpha(\log P - 1.18) + \beta$.

Band	Galaxy	α	$\sigma(\alpha)$	β	$\sigma(\beta)$	Std.dev.	ΔM
M_K	SMC	−3.247	0.141	−6.077	0.046	0.24	0.148
M_K	LMC	−3.247	0.088	−6.225	0.036	0.21	0.000
M_K	MW	−3.247	0.092	−6.267	0.030	0.23	−0.042
M_J	SMC	−3.156	0.177	−5.595	0.058	0.31	0.155
M_J	LMC	−3.156	0.091	−5.750	0.037	0.22	0.000
M_J	MW	−3.156	0.092	−5.807	0.030	0.23	−0.057
W_{JK}	SMC	−3.360	0.133	−6.406	0.043	0.23	0.147
W_{JK}	LMC	−3.360	0.089	−6.552	0.036	0.21	0.000
W_{JK}	MW	−3.360	0.097	−6.589	0.032	0.24	−0.037
M_V	SMC	−2.690	0.177	−4.239	0.057	0.30	0.260
M_V	LMC	−2.690	0.112	−4.498	0.045	0.27	0.000
M_V	MW	−2.690	0.100	−4.465	0.033	0.25	0.033
M_I	SMC	−2.911	0.156	−5.065	0.051	0.27	0.206
M_I	LMC	−2.911	0.103	−5.270	0.042	0.22	0.000
M_I	MW	−2.911	0.104	−5.320	0.033	0.22	−0.050
W_{VI}	SMC	−3.320	0.148	−6.336	0.048	0.26	0.140
W_{VI}	LMC	−3.320	0.114	−6.476	0.046	0.24	0.000
W_{VI}	MW	−3.320	0.121	−6.588	0.038	0.26	−0.112
				mag	mag	mag	mag

and I bands, we adopted the reference slopes from the OGLE samples determined by Soszyński et al. (2015) of −2.690 ± 0.018, and −2.911 ± 0.014. For the Wesenheit $V,(V-I)$ index we adopted −3.32 ± 0.08 from Storm et al. (2011a). In the J and K band we adopted the values from Macri et al. (2015) of −3.156 ± 0.004 and −3.247 ± 0.004, respectively, which also agrees very well with the relations from Persson et al. (2004). For W_{JK}we adopted a value of −3.36 ± 0.1 based on the Milky Way sample from Table 7.

Our adopted PL relation slope values agree quite well with other modern determinations (e.g., Subramanian & Subramaniam 2015; Macri et al. 2015; Bhardwaj et al. 2016; Inno et al. 2016; Ripepi et al. 2017). Small nonlinearities of the LMC PL relations in different optical bands at around 10 d have been reported by Tammann et al. (2003), Kanbur & Ngeow (2004), Bhardwaj et al. (2016), and references therein. There might also be a small nonlinearity in PL relations in near-infrared bands (Bhardwaj et al. 2016). These nonlinearities are so small, however, that they do not affect our conclusions in any significant way. We are also aware of the fact that the Magellanic Cloud PL relations in the literature, like those based on the OGLE samples, are based on Cepheid samples that contain a much larger number of short-period Cepheids than Cepheids with periods longer than 10 d. However, cutting out the short-period Cepheids in the PL relation solutions does not significantly change the slopes. An important consideration is also that Cepheid samples detected in distant galaxies (beyond several Mpc), which are important in the context of the determination of the Hubble constant, always consist of long-period Cepheids because the short-period variables are too faint to be detected.

We plot in Fig. 9 the zero point offsets from Table 8 against the adopted metallicity values from Sect. 4. To obtain realistic error estimates we used the Python package `emcee` (Foreman-Mackey et al. 2013) to perform Markov chain Monte Carlo simulations based on a linear model between metallicity and the magnitude offset, including the estimated errors on both parameters. Following the discussion in Sect. 2.5 we added in quadrature to the statistical errors the contribution from the uncertainty in the zero points of the reddening scales, $\sigma_{\rm sys}(M_\lambda) = R_\lambda \times \sigma_{\rm sys}(E(B-V))$, where R_λ is the ratio of total to selective absorption, as given in Sect. 2.5, and $\sigma_{\rm sys}(E(B-V)) = 0.05$ mag. The lines overplotted in the figures are the resulting relations which are listed with their associated errors in Table 9. In W_{VI}we find a linear relation with a slope of -0.34 ± 0.06 mag dex^{-1}. In the K band we also find a significant variation from SMC to MW metallicity with a slope of -0.23 ± 0.06 mag dex^{-1} in the sense that metal-poor stars are fainter than metal-rich stars for a given pulsation period. From Fig. 9 it can also be seen that the relation might not be entirely linear in all bands, but might be steeper for lower metallicities.

6. Discussion

Storm et al. (2011a) calibrated the p-factor relation for the IRSB method to give distances independent of pulsation period and in agreement with the Benedict et al. (2007) HST parallaxes to nine galactic Cepheids. The LMC distance modulus that results from the mean of the individual distances to the sample of LMC Cepheids is $(m-M)_0 = 18.46 \pm 0.04$ (statistical only), which is in excellent agreement with the very accurate modulus of $(m-M)_0 = 18.493 \pm 0.047$ (statistical and systematic) determined by Pietrzyński et al. (2013) from late-type eclipsing binaries. The zero point of the method thus seems to be very well established. We note that in the present work we are only looking for differential effects with metallicity so any shift of the absolute zero point will have little impact, if any, on the conclusions.

As already discussed in Sect. 3, the effect of metallicity on the method itself is also very small. Metallicity could potentially affect the p-factor relation as well as the surface brightness-color relation. Nardetto et al. (2011) showed that the p-factor is largely independent of the metallicity and Thompson et al. (2001) showed that the effect on the surface brightness $(V-K)$ relation is also very small. Similarly, Storm et al. (2004b) showed that the method itself is robust to metallicity variations. Furthermore, any changes in either the adopted p-factor relation or the surface brightness-color relation would affect all three samples in equal measure and would not significantly change the result.

Apart from the method itself, we also have to consider systematic differences between our samples, in particular that the reddening and metallicities are on the same scale. As already explained in Sect. 3, the method is very robust to errors in the reddening (an error of 0.05 mag leads to an error in the distance modulus of 0.025 mag). Reddening errors, however, carry over directly in the luminosities so reddening insensitive indices perform much better as distance indicators. We have included the estimated systematic uncertainties in the reddenings in the fits of the metallicity effect and it can be seen in Table 9 that the reddening insensitive indices are indeed very well constrained.

The metallicity scales as described in Sect. 4 also appear to be in very good agreement and we find the possible systematic difference to be less than 0.03 dex, which has been included in the error propagation.

We are thus confident that the derived absolute magnitudes are all on the same system and that the offsets in the zero points as determined in Sect. 5 are real and significant. We also note here that the metallicity effects found in Sect. 5 do not in any way rely on an ensemble distance to either the LMC or the SMC, but rely on the individual distance estimates for each star. We are thus entirely free of influence from any depth effects in the clouds. The main remaining limitation is that we still rely on mean metallicity values for each sample.

The new data presented here allow us for the first time to determine the PL relations directly for SMC Cepheids. We now

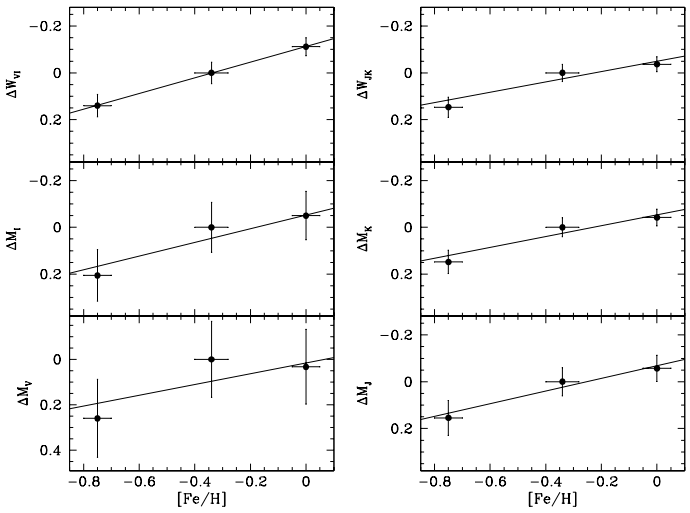

Fig. 9. Luminosity zero point offsets in the different passbands as a function of the metallicity of each of the samples (SMC, LMC, and MW) with the associated error bars from Table 8. The metallicities and their error bars are taken from Sect. 4 and the lines represent the statistically most plausible model.

Table 9. Relation of ΔM vs. [Fe/H] for the various bands in the form $\Delta M = \gamma$[Fe/H] + ψ.

Band	γ	$\sigma(\gamma)$	ψ	$\sigma(\psi)$
M_J	−0.270	0.108	−0.068	0.044
M_K	−0.232	0.064	−0.054	0.024
W_{JK}	−0.221	0.053	−0.049	0.019
M_V	−0.238	0.186	0.016	0.111
M_I	−0.293	0.150	−0.053	0.076
W_{VI}	−0.335	0.059	−0.113	0.023
	mag dex^{-1}	mag dex^{-1}	mag	mag

Notes. The fitting errors $\sigma(\gamma)$ and $\sigma(\psi)$ based on Markov chain Monte Carlo analysis is given as well.

have SMC and LMC samples of comparable size and spanning the full range of periods for classical fundamental mode Cepheids. The slopes are in excellent agreement with the slopes for the LMC and MW samples and the large sample allows us to constrain much more accurately the metal-poor magnitude zero point, as was the case in Storm et al. (2011b). The estimated uncertainties on the metallicity effect are now pushed down to 0.06 mag dex^{-1}, or almost half of the value we obtained previously. The effect is now somewhat stronger than reported there, and it is much more significant due to the reduced uncertainty. We note that the relations do not appear perfectly linear and that there might be a stronger effect in the metal-poor regime. The data is still consistent with a negligible effect for metallicities in the range from −0.35 to 0.0. However, the metal-poor data point puts a very strong constraint on the slope that is hardly possible with the significantly smaller metal range covered by LMC and MW Cepheids.

Due to our significant sample size and the distribution of the Cepheids across the face of the SMC we believe that we can determine a reasonable distance to the SMC itself even though the SMC exhibits significant depth effects (see, e.g., Ripepi et al. 2017, Muraveva et al. 2018). In this way we can also determine the difference in distance modulus between the two clouds. In Sect. 5 we found a difference of $\Delta(m - M)_0 = 0.40$ mag. This compares very well with the value of 0.44 ± 0.10 mag determined by Cioni et al. (2000) via the "Tip of the Red Giant Branch" method in IJK bands, the value of 0.458 ± 0.068 mag determined by Graczyk et al. (2014) from a combination of indicators (Cepheids, RR Lyr, Red clump, and eclipsing binaries), and the value of 0.39 ± 0.05 mag derived by Szewczyk et al. (2009) from near-infrared photometry of RR Lyrae variables. The much elongated structure of the SMC along the line of sight, with a range of 10 kpc from RR Lyrae stars (Muraveva et al. 2018) and an even wider range from the Cepheids (Ripepi et al. 2017) complicates the determination of a sensible mean distance to the SMC, but at least we can conclude that our IRSB-based distances to the Cepheids in our LMC and SMC samples compare very well with the results obtained from other distance indicators applied in a purely differential way. We note here that the observed dispersion around the SMC PL relation in the K band of 0.24 mag corresponds to a depth effect of 6 kpc, but this dispersion is identical to what we observe for the LMC and MW samples, suggesting that depth effects are not significantly affecting our results.

Most of the previous observational determinations of the metallicity effect on the Cepheid PL relation used the "inner/outer field method", where magnitudes of Cepheid samples in a field close to the center of a spiral galaxy were compared to the magnitudes of their Cepheid counterparts in a field located at a much larger galactocentric distance. In all such studies the inner-field Cepheids were found to be brighter than the more metal-poor outer field Cepheids leading, together with an adopted metallicity gradient in the disk of the galaxy, to a negative sign of the metallicity effect, as in our present study. There are, however, two fundamental problems with this approach. First, there are a number of calibrations of H II region oxygen abundances in the literature yielding quite different results, so the size of the derived metallicity effect depends on the adopted oxygen abundance calibration (e.g., Bresolin et al. 2009). Second, Cepheids in the inner fields are more strongly affected by crowding and blending problems, so at least part of the systematically brighter magnitudes of inner field Cepheids may be caused by close companion stars which are not resolved in the photometry. An example is the excellent work of Shappee & Stanek (2011), who find a metallicity effect of −0.80 mag dex^{-1} in optical V and I bands in M 101 using HST/ACS images, which seems to be unreasonably large and is probably significantly biased by crowding affecting the Cepheids in their inner field in M 101. Deriving the metallicity effect in nearby galaxies like the Magellanic Clouds where crowding is not a problem in the photometry seems therefore to be a safer way to determine the true size and sign of the Cepheid metallicity effect.

It is particularly interesting to compare the metallicity effect we obtain in this study with the recent determination reported by Wielgórski et al. (2017) who used a completely different approach and basically obtained a zero effect in all bands. Their determination critically depends on the distance difference between LMC and SMC which they assume to be 0.472 ± 0.026 mag, as obtained from similar late-type eclipsing binary systems in both galaxies. While the LMC distance obtained from this method is extremely well established (Pietrzyński et al. 2013), the SMC distance reported in Graczyk et al. (2014) is based on only five systems. The average distance modulus obtained from this small number of systems might not represent the SMC mean distance very well considering the large spread of the SMC in the line of sight we discussed before. A change of 0.07 mag in the mean SMC distance, from the 18.97 mag value obtained by Graczyk et al. (2014) to 18.90 mag, might thus be consistent with the current uncertainty on the eclipsing binary distance to the SMC. If the conjecture is correct, it would bring

the metallicity effect determination in Wielgórski et al. (2017) to about -0.2 mag dex^{-1} in all bands, in excellent agreement with the value derived in this paper. We therefore suspect that the apparent discrepancy between the zero metallicity effect found by Wielgórski et al. (2017), and the -0.2 mag dex^{-1} effect found in this paper, is due to an overestimated SMC distance in Graczyk et al. (2014) from their small number of systems available for analysis.

7. Conclusions

We obtained new and very accurate radial velocity and K-band light curves of 26 SMC Cepheids, expanding our previous sample of five stars reported in Storm et al. (2004b, 2011b) to 31 Cepheids covering the full Cepheid period range from 4 to 69 days. We complemented our new K-band light curves with data from the VMC Survey. Using these data together with the excellent V-band light curves of the variables from the OGLE Project, we applied the IRSB Technique as calibrated by Storm et al. (2011a) and calculated the distances of the individual SMC Cepheids, and their absolute magnitudes in near-infrared and optical bands. These magnitudes define tight PL relations in the V, I, J, and K bands and in the optical and near-infrared Wesenheit indices, with dispersions practically identical to the relations we previously obtained with the same technique for Cepheid samples in the Milky Way and LMC and reported in Storm et al. (2011b).

We find very good agreement between the slopes of these PL relations and the fiducial PL relations in the LMC obtained by Soszyński et al. (2015) in the optical, and by Macri et al. (2015) in the near-infrared bands, supporting the universality of the slopes of Cepheid PL relations in these wavelength regimes. Our SMC Cepheid distances yield a mean SMC distance of 18.86 ± 0.04 mag which compares very well with recent determinations from other distance indicators. From the Cepheid samples analyzed with the IRSB Technique in the LMC and SMC we obtain a distance difference between the Clouds of 0.40 mag, which again compares very well to other recent estimates from different standard candles. The distance modulus of 18.46 ± 0.04 mag we obtain for the LMC from our Cepheid sample in this galaxy is in excellent agreement with the near-geometrical value of 18.497 mag established by Pietrzyński et al. (2013) from late-type eclipsing binaries.

We find that the absolute PL relations defined by the SMC Cepheids are significantly displaced to fainter magnitudes compared to their MW and LMC counterparts. This is true for all near-infrared and optical bands studied in this paper, and argues for a metallicity effect in all bands in the sense that the more metal-poor Cepheids are intrinsically fainter than their more metal-rich counterparts with similar pulsation periods. The metallicity effect we obtain is -0.23 ± 0.06 mag dex^{-1} in the near-infrared K band, and slightly larger in the J, I, and the optical Wesenheit bands. The uncertainties have been reduced by almost a factor of two with respect to our previous work and the effect is now very significant (3σ). Our data suggests that the change in the PL relation zero points with metallicity might not be entirely linear in the different studied bands, but might become steeper for lower metallicities. We note that our IRSB analyses of the Cepheids in the MW, LMC, and SMC samples were carried out following identical procedures leading to a strictly differential analysis between the absolute magnitudes of the Cepheids in the three galaxies, making our results and conclusions independent of eventual systematic errors on the distances due to imperfections in the technique. We have also shown that there is no systematic offset between the reddening scales adopted for the SMC Cepheids in the present work, and for the LMC Cepheids in our previous work, which combined with the reddening insensitivity of the method itself means that reddening effects on the final relations for the K-band and Wesenheit indices are negligble.

We argue that the K-band Cepheid PL relation continues to be the best tool for determining the distances to late-type galaxies. However, the mild but significant metallicity effect determined in this paper should be taken into account, which obviously requires an estimate of the average metallicities of the Cepheid samples used in such determinations.

Acknowledgements. W.G. and G.P. gratefully acknowledge financial support for this work from the BASAL Centro de Astrofisica y Tecnologias Afines (CATA) AFB-170002. W.G., D.G., and M.G. also gratefully acknowledge financial support from the Millenium Institute of Astrophysics (MAS) of the Iniciativa Cientifica Milenio del Ministerio de Economia, Fomento y Turismo de Chile, Project IC120009. This research has also been supported by funding from the European Union's 2020 research and innovation program (grant agreement No. 695099). Support from IdP II 2015 0002 64 grant of the Polish Ministry of Science and Higher Education is also acknowledged. We are greatly indebted to the staff at the European Southern Observatory La Silla and Paranal sites, and the staff at Las Campanas Observatory, for their excellent support during the many visitor mode runs which allowed us to collect the data for this study. We are pleased to thank ESO and the Chilean TAC for the large amounts of observing time allotted to this program.

References

Alonso-García, J., Minniti, D., Catelan, M., et al. 2017, ApJ, 849, L13
Anderson, R. I. 2016, MNRAS, 463, 1707
Andrievsky, S. M., Egorova, I. A., Korotin, S. A., & Kovtyukh, V. V. 2003, Astron. Nachr., 324, 532
Barnes, T. G., & Evans, D. S. 1976, MNRAS, 174, 489
Barnes, III., T. G., Storm, J., Jefferys, W. H., Gieren, W. P., & Fouqué, P. 2005, ApJ, 631, 572
Benedict, G. F., McArthur, B. E., Feast, M. W., et al. 2007, AJ, 133, 1810
Bernstein, R., Shectman, S. A., Gunnels, S. M., Mochnacki, S., & Athey, A. E. 2003, Proc. SPIE, 4841, 1694
Bhardwaj, A., Kanbur, S. M., Macri, L. M., et al. 2016, MNRAS, 457, 1644
Bono, G., Caputo, F., Fiorentino, G., Marconi, M., & Musella, I. 2008, ApJ, 684, 102
Boyajian, T. S., von Braun, K., van Belle, G., et al. 2013, ApJ, 771, 40
Bresolin, F., Gieren, W., Kudritzki, R.-P., et al. 2009, ApJ, 700, 309
Caputo, F., Marconi, M., Musella, I., & Santolamazza, P. 2000, A&A, 359, 1059
Cardelli, J. A., Clayton, G. C., & Mathis, J. S. 1989, ApJ, 345, 245
Carpenter, J. M. 2001, AJ, 121, 2851
Carter, B. S. 1990, MNRAS, 242, 1
Challouf, M., Nardetto, N., Mourard, D., et al. 2014, A&A, 570, A104
Cioni, M.-R. L., van der Marel, R. P., Loup, C., & Habing, H. J. 2000, A&A, 359, 601
Cioni, M.-R. L., Clementini, G., Girardi, L., et al. 2011, A&A, 527, A116
Coelho, P., Barbuy, B., Meléndez, J., Schiavon, R. P., & Castilho, B. V. 2005, A&A, 443, 735
Dekker, H., D'Odorico, S., Kaufer, A., Delabre, B., & Kotzlowski, H. 2000, Proc. SPIE, 4008, 534
Fausnaugh, M. M., Kochanek, C. S., Gerke, J. R., et al. 2015, MNRAS, 450, 3597
Foreman-Mackey, D., Hogg, D. W., Lang, D., & Goodman, J. 2013, PASP, 125, 306
Fouqué, P., & Gieren, W. P. 1997, A&A, 320, 799
Fouqué, P., Arriagada, P., Storm, J., et al. 2007, A&A, 476, 73
Freedman, W. L., & Madore, B. F. 2011, ApJ, 734, 46
Freedman, W. L., Madore, B. F., Gibson, B. K., et al. 2001, ApJ, 553, 47
Freudling, W., Romaniello, M., Bramich, D. M., et al. 2013, A&A, 559, A96
Fry, A. M., & Carney, B. W. 1997, AJ, 113, 1073
Gaia Collaboration (Clementini, G., et al.) 2017, A&A, 605, A79
Gallenne, A., Kervella, P., Mérand, A., et al. 2017, A&A, 608, A18
Genovali, K., Lemasle, B., Bono, G., et al. 2014, A&A, 566, A37
Gieren, W. P., Barnes, III., T. G., & Moffett, T. J. 1993, ApJ, 418, 135
Gieren, W. P., Fouqué, P., & Gómez, M. 1997, ApJ, 488, 74
Gieren, W. P., Fouqué, P., & Gómez, M. 1998, ApJ, 496, 17

Gieren, W., Storm, J., Barnes, III., T. G., et al. 2005, ApJ, 627, 224
Gould, A. 1994, ApJ, 426, 542
Graczyk, D., Pietrzyński, G., Thompson, I. B., et al. 2012, ApJ, 750, 144
Graczyk, D., Pietrzyński, G., Thompson, I. B., et al. 2014, ApJ, 780, 59
Graczyk, D., Konorski, P., Pietrzyński, G., et al. 2017, ApJ, 837, 7
Graczyk, D., Pietrzyński, G., Thompson, I. B., et al. 2018, ApJ, 860, 1
Groenewegen, M. A. T. 2013, A&A, 550, A70
Haschke, R., Grebel, E. K., & Duffau, S. 2011, AJ, 141, 158
Hawarden, T. G., Leggett, S. K., Letawsky, M. B., Ballantyne, D. R., & Casali, M. M. 2001, MNRAS, 325, 563
Imbert, M., Andersen, J., Ardeberg, A., et al. 1989, A&AS, 81, 339
Inno, L., Bono, G., Matsunaga, N., et al. 2016, ApJ, 832, 176
Kanbur, S. M., & Ngeow, C.-C. 2004, MNRAS, 350, 962
Kelson, D. D. 2003, PASP, 115, 688
Kennicutt, Jr., R. C., Stetson, P. B., Saha, A., et al. 1998, ApJ, 498, 181
Kervella, P., Bersier, D., Mourard, D., et al. 2004, A&A, 428, 587
Kervella, P., Trahin, B., Bond, H. E., et al. 2017, A&A, 600, A127
Laney, C. D., & Stobie, R. S. 1986, S. Afr. Astron. Obs. Circ., 10, 51
Lemasle, B., François, P., Genovali, K., et al. 2013, A&A, 558, A31
Lemasle, B., Groenewegen, M. A. T., Grebel, E. K., et al. 2017, A&A, 608, A85
Luck, R. E., & Lambert, D. L. 2011, AJ, 142, 136
Luck, R. E., Moffett, T. J., Barnes, III., T. G., & Gieren, W. P. 1998, AJ, 115, 605
Luck, R. E., Andrievsky, S. M., Kovtyukh, V. V., Gieren, W., & Graczyk, D. 2011, AJ, 142, 51
Macri, L. M., Ngeow, C.-C., Kanbur, S. M., Mahzooni, S., & Smitka, M. T. 2015, AJ, 149, 117
Mager, V. A., Madore, B. F., & Freedman, W. L. 2013, ApJ, 777, 79
Mayor, M., Pepe, F., Queloz, D., et al. 2003, The Messenger, 114, 20
Mérand, A., Kervella, P., Breitfelder, J., et al. 2015, A&A, 584, A80
Molinaro, R., Ripepi, V., Marconi, M., et al. 2012, ApJ, 748, 69
Moorwood, A., Cuby, J.-G., & Lidman, C. 1998, The Messenger, 91, 9
Muraveva, T., Subramanian, S., Clementini, G., et al. 2018, MNRAS, 473, 3131
Nardetto, N., Fokin, A., Fouqué, P., et al. 2011, A&A, 534, L16
Nardetto, N., Poretti, E., Rainer, M., et al. 2017, A&A, 597, A73
Persson, S. E., Madore, B. F., Krzemiński, W., et al. 2004, AJ, 128, 2239
Pietrzyński, G., & Gieren, W. 2002, AJ, 124, 2633
Pietrzyński, G., Gieren, W., & Udalski, A. 2002, PASP, 114, 298
Pietrzyński, G., Graczyk, D., Gieren, W., et al. 2013, Nature, 495, 76
Pilecki, B., Gieren, W., Smolec, R., et al. 2017, ApJ, 842, 110
Pilecki, B., Gieren, W., Pietrzyński, G., et al. 2018, ApJ, 862, 43
Riess, A. G., Macri, L. M., Hoffmann, S. L., et al. 2016, ApJ, 826, 56
Riess, A. G., Casertano, S., Yuan, W., et al. 2018, ApJ, 855, 136
Ripepi, V., Marconi, M., Moretti, M. I., et al. 2016, ApJS, 224, 21
Ripepi, V., Cioni, M.-R. L., Moretti, M. I., et al. 2017, MNRAS, 472, 808
Romaniello, M., Primas, F., Mottini, M., et al. 2008, A&A, 488, 731
Rucinski, S. 1999, ASP Conf. Ser., 185, 82
Rucinski, S. M. 1992, AJ, 104, 1968
Sakai, S., Ferrarese, L., Kennicutt, Jr., R. C., & Saha, A. 2004, ApJ, 608, 42
Sandage, A., Tammann, G. A., Saha, A., et al. 2006, ApJ, 653, 843
Shappee, B. J., & Stanek, K. Z. 2011, ApJ, 733, 124
Soszyński, I., Poleski, R., Udalski, A., et al. 2008, Acta Astron., 58, 163
Soszyński, I., Udalski, A., Szymański, M. K., et al. 2015, Acta Astron., 65, 297
Stetson, P. B. 1987, PASP, 99, 191
Stetson, P. B. 1994, PASP, 106, 250
Storm, J., Carney, B. W., Gieren, W. P., et al. 2004a, A&A, 415, 521
Storm, J., Carney, B. W., Gieren, W. P., et al. 2004b, A&A, 415, 531
Storm, J., Gieren, W., Fouqué, P., et al. 2011a, A&A, 534, A94
Storm, J., Gieren, W., Fouqué, P., et al. 2011b, A&A, 534, A95
Subramanian, S., & Subramaniam, A. 2015, A&A, 573, A135
Szewczyk, O., Pietrzyński, G., Gieren, W., et al. 2009, AJ, 138, 1661
Tammann, G. A., Sandage, A., & Reindl, B. 2003, A&A, 404, 423
Thompson, I. B., Kaluzny, J., Pych, W., et al. 2001, AJ, 121, 3089
Turner, D. G. 2016, Rev. Mex. Astron. Astrofis., 52, 223
Udalski, A., Soszyński, I., Szymański, M. K., et al. 2008, Acta Astron., 58, 329
Udalski, A., Szymański, M. K., & Szymański, G. 2015, Acta Astron., 65, 1
Welch, D. L. 1994, AJ, 108, 1421
Welch, D. L., McLaren, R. A., Madore, B. F., & McAlary, C. W. 1987, ApJ, 321, 162
Wielgórski, P., Pietrzyński, G., Gieren, W., et al. 2017, ApJ, 842, 116

Appendix A: Light and radial velocity curves

In Figs. A.1–A.26 we show the data used for the IRSB analysis as described in Sect. 2 for each of the stars. In the K-band light curve we distinguish between the new data presented here (filled circles) and the appropriately shifted VMC data (open circles). The adopted Fourier fit to the K-band light curve has also been overplotted.

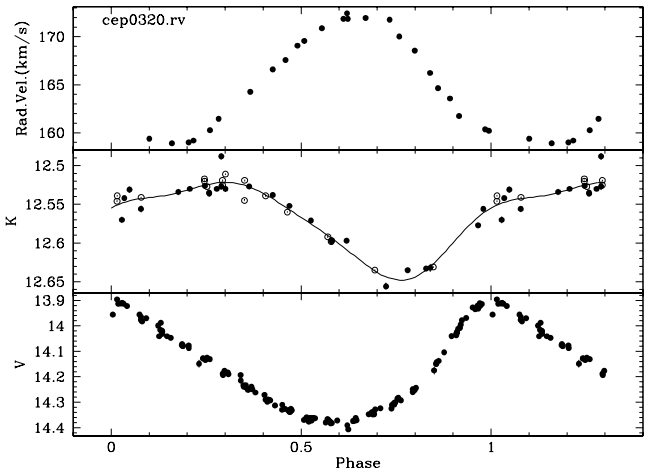

Fig. A.1. Light and radial velocity curves for the star OGLE-SMC-CEP0320.

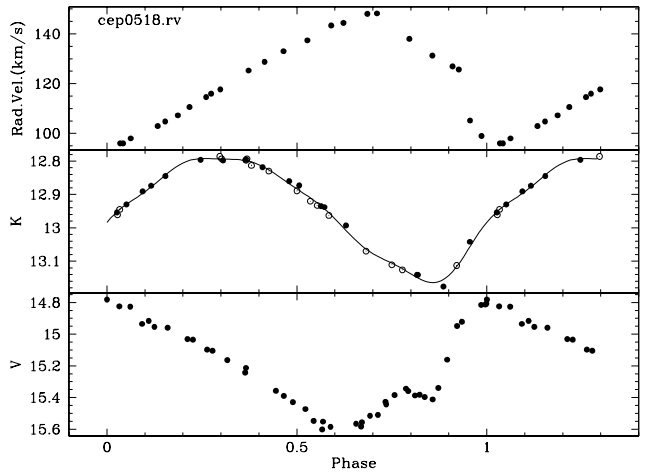

Fig. A.2. Light and radial velocity curves for the star OGLE-SMC-CEP0518.

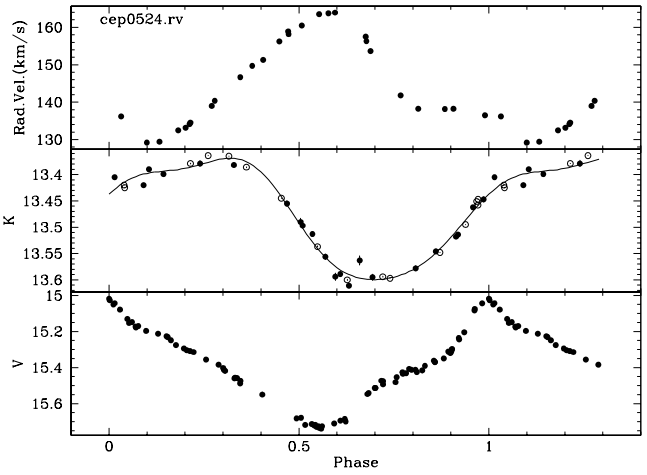

Fig. A.3. Light and radial velocity curves for the star OGLE-SMC-CEP0524.

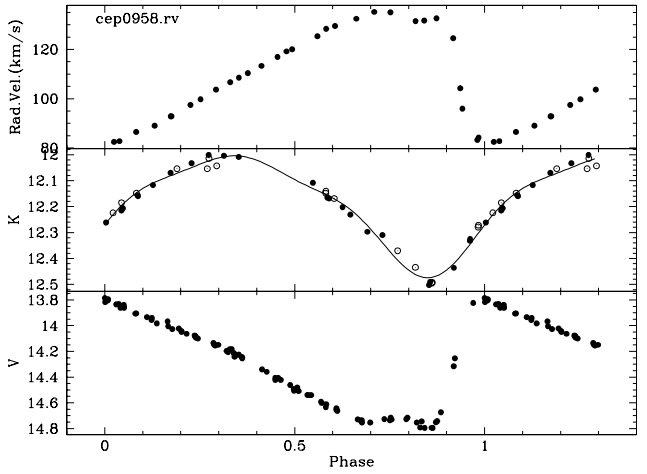

Fig. A.4. Light and radial velocity curves for the star OGLE-SMC-CEP0958.

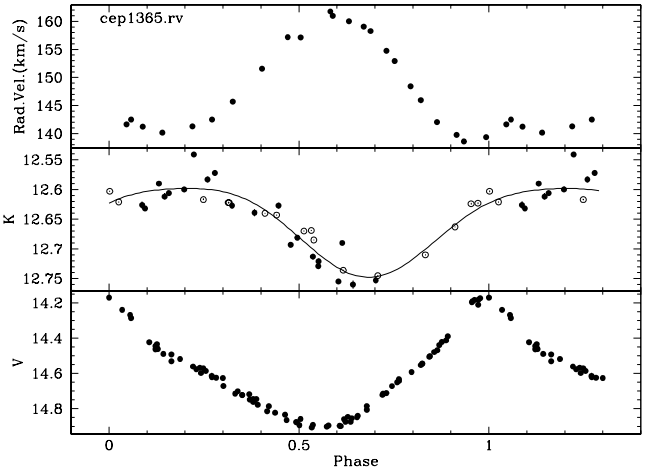

Fig. A.5. Light and radial velocity curves for the star OGLE-SMC-CEP1365.

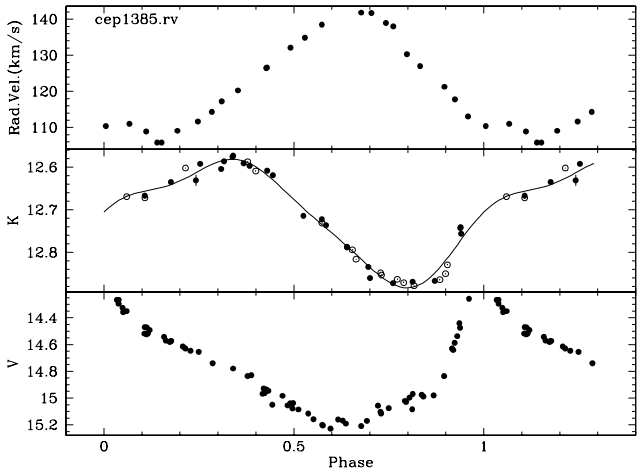

Fig. A.6. Light and radial velocity curves for the star OGLE-SMC-CEP1385.

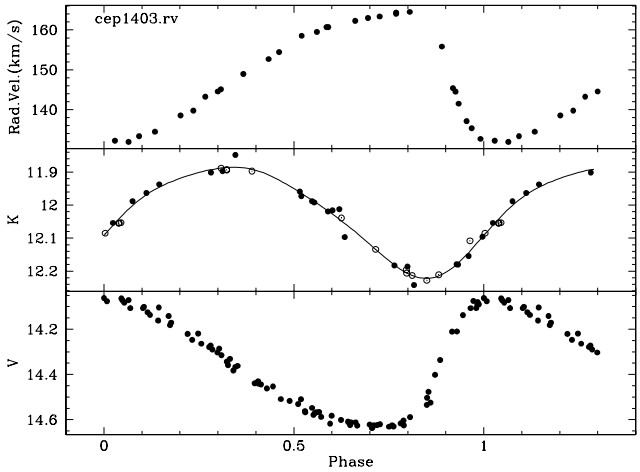

Fig. A.7. Light and radial velocity curves for the star OGLE-SMC-CEP1403.

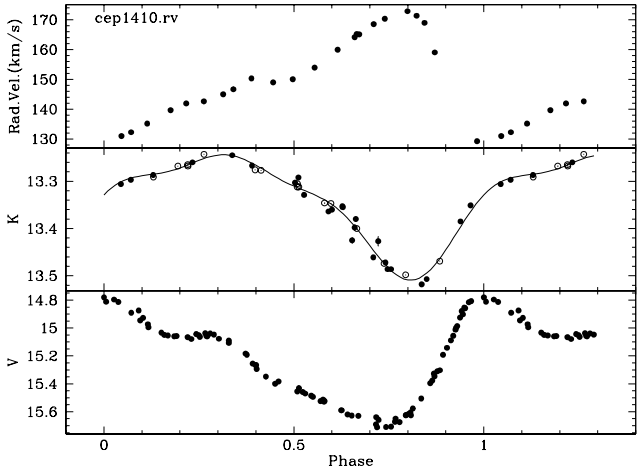

Fig. A.8. Light and radial velocity curves for the star OGLE-SMC-CEP1410.

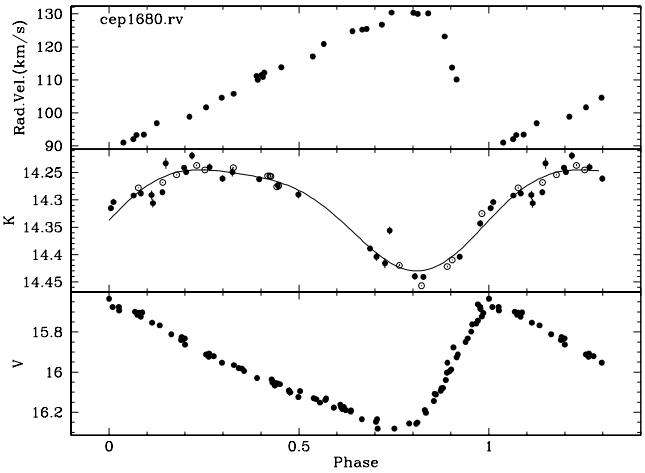

Fig. A.9. Light and radial velocity curves for the star OGLE-SMC-CEP1680.

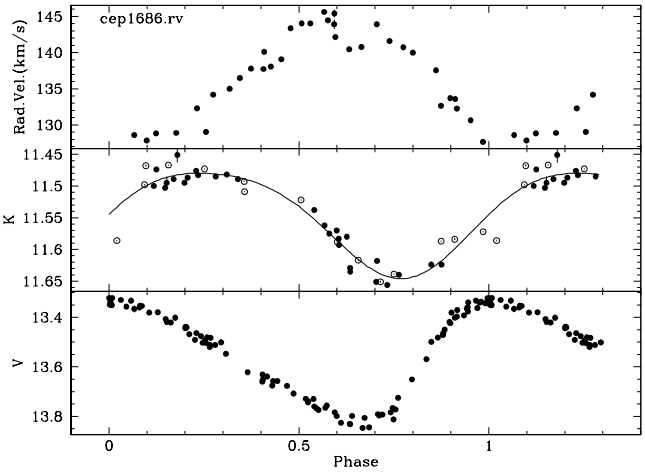

Fig. A.10. Light and radial velocity curves for the star OGLE-SMC-CEP1686.

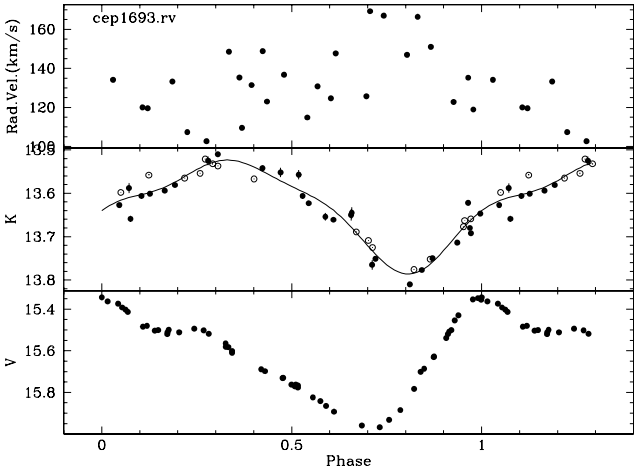

Fig. A.11. Light and radial velocity curves for the star OGLE-SMC-CEP1693.

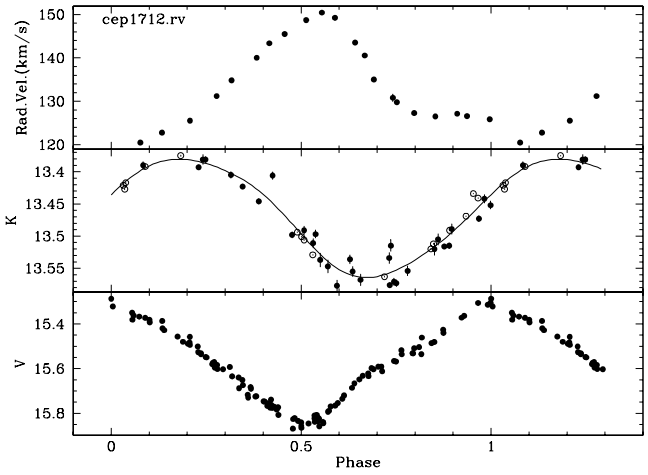

Fig. A.12. Light and radial velocity curves for the star OGLE-SMC-CEP1712.

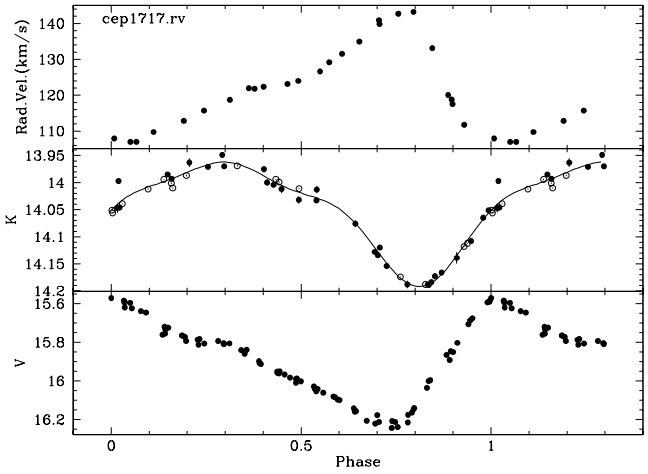

Fig. A.13. Light and radial velocity curves for the star OGLE-SMC-CEP1717.

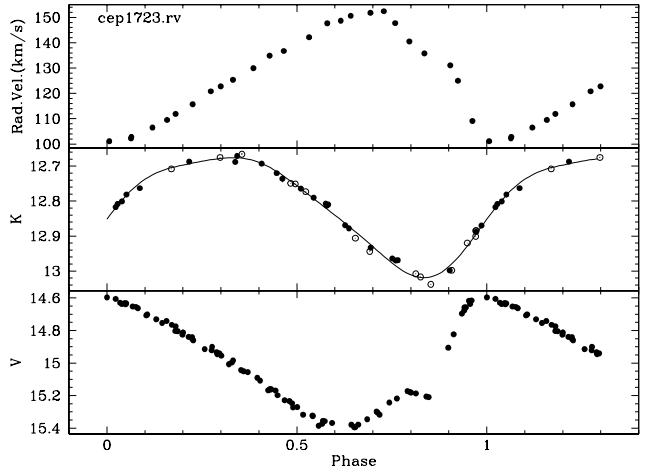

Fig. A.14. Light and radial velocity curves for the star OGLE-SMC-CEP1723.

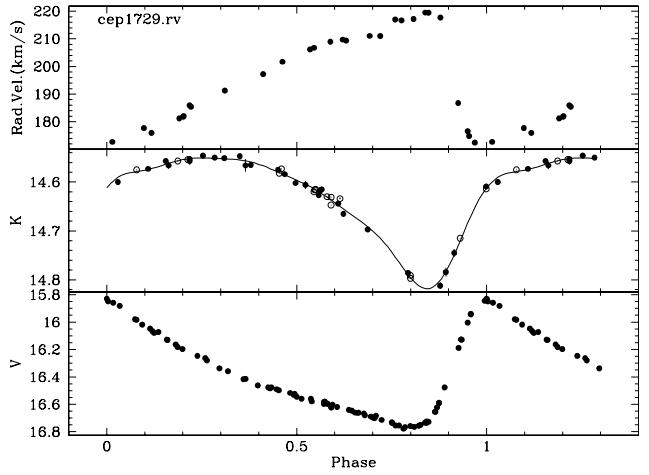

Fig. A.15. Light and radial velocity curves for the star OGLE-SMC-CEP1729.

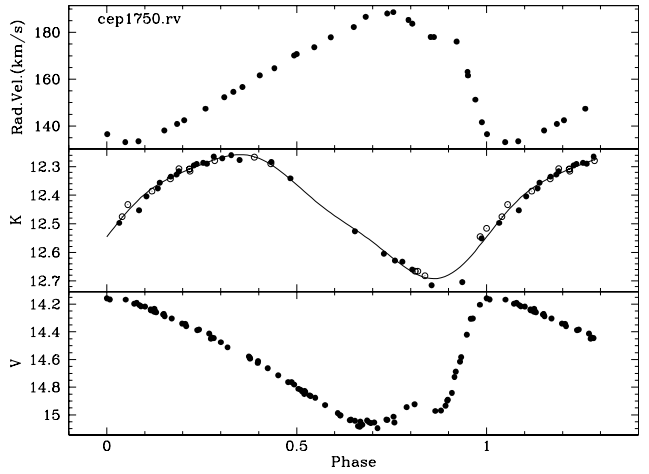

Fig. A.16. Light and radial velocity curves for the star OGLE-SMC-CEP1750.

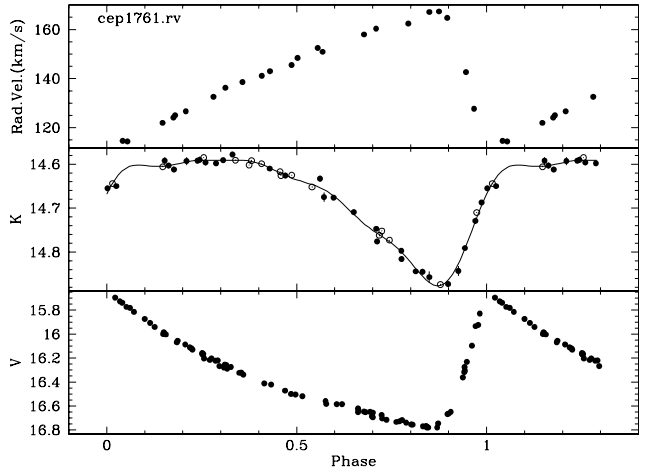

Fig. A.17. Light and radial velocity curves for the star OGLE-SMC-CEP1761.

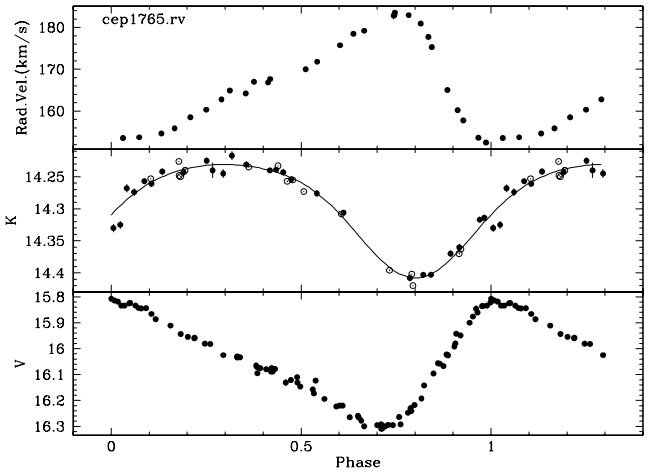

Fig. A.18. Light and radial velocity curves for the star OGLE-SMC-CEP1765.

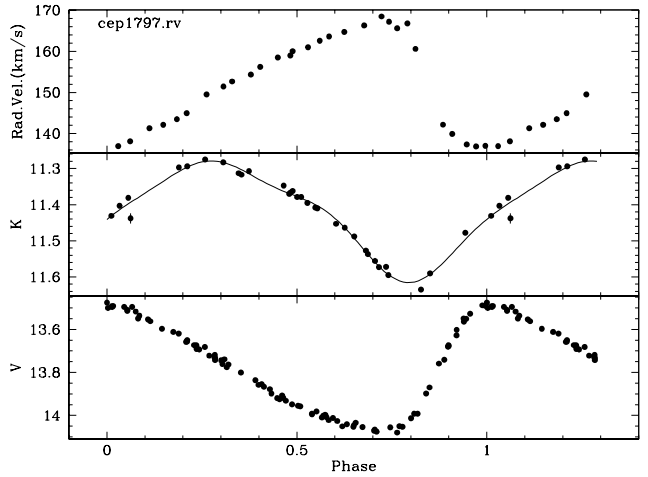

Fig. A.19. The light and radial velocity curves for the star OGLE-SMC-CEP1797.

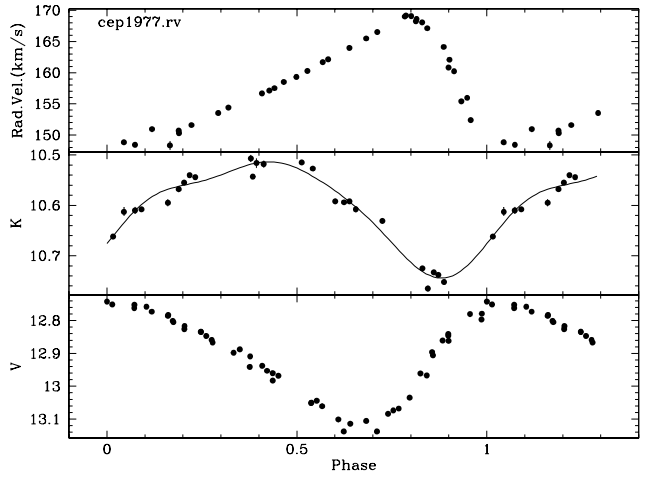

Fig. A.20. Light and radial velocity curves for the star OGLE-SMC-CEP1977.

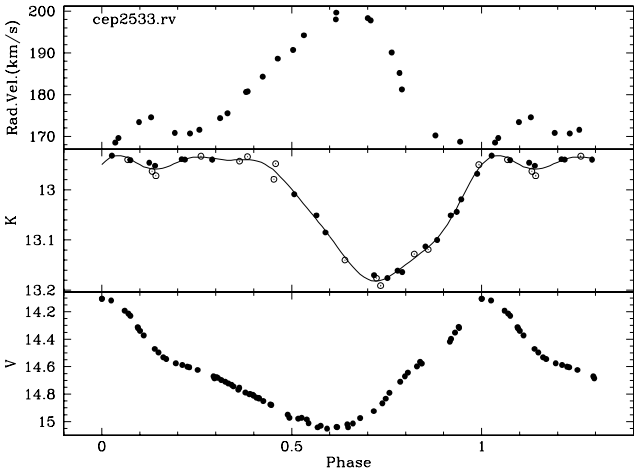

Fig. A.21. The light and radial velocity curves for the star OGLE-SMC-CEP2533.

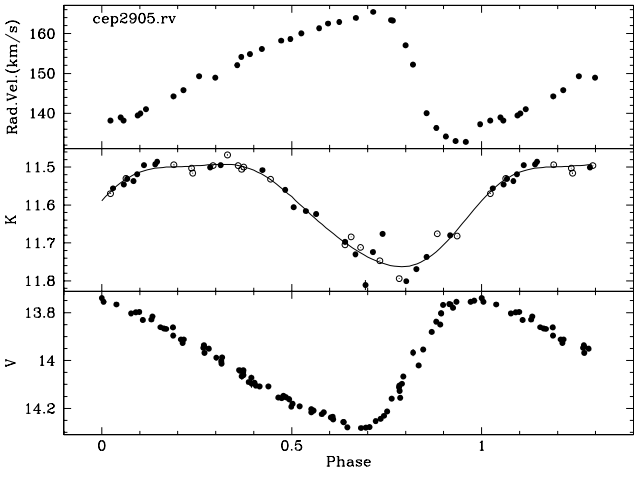

Fig. A.22. Light and radial velocity curves for the star OGLE-SMC-CEP2905.

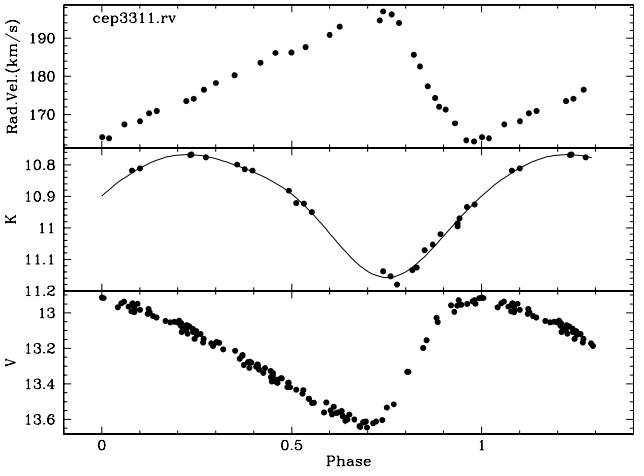

Fig. A.23. The light and radial velocity curves for the star OGLE-SMC-CEP3311.

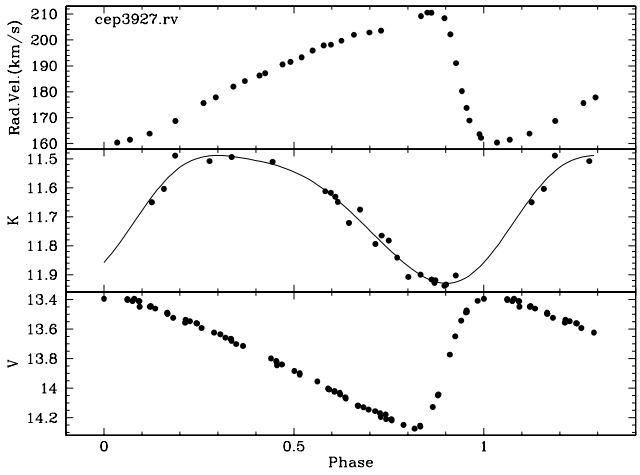

Fig. A.24. Light and radial velocity curves for the star OGLE-SMC-CEP3927.

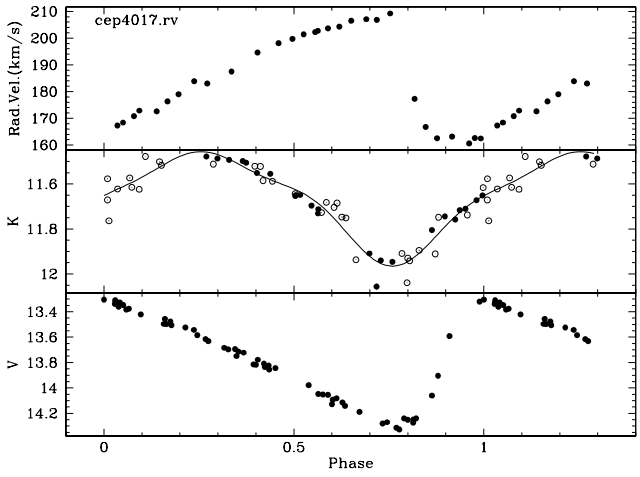

Fig. A.25. The light and radial velocity curves for the star OGLE-SMC-CEP4017.

Appendix B: Removing orbital motion from the radial velocity curves

In Sect. 2.6 it was shown that some of the stars exhibit secular radial velocity changes which are most likely due to orbital motion. We have attempted to minimize the impact of these secular drifts by applying velocity offsets to data from different time intervals by trying to obtain continous radial velocity curves as a function of phase and also assuming that such drifts are slow compared to the pulsational period of the stars. In Figs. B.1–B.5 we have plotted the observed data (upper panels), the corrected data (middle panels), and the applied radial velocity offsets (lower panels). The symbols correspond to certain time intervals and we have estimated the offsets in steps of $1\,\mathrm{km\,s^{-1}}$. It can be seen that the scatter around the radial velocity curves are strongly reduced, and from the lower panels it can

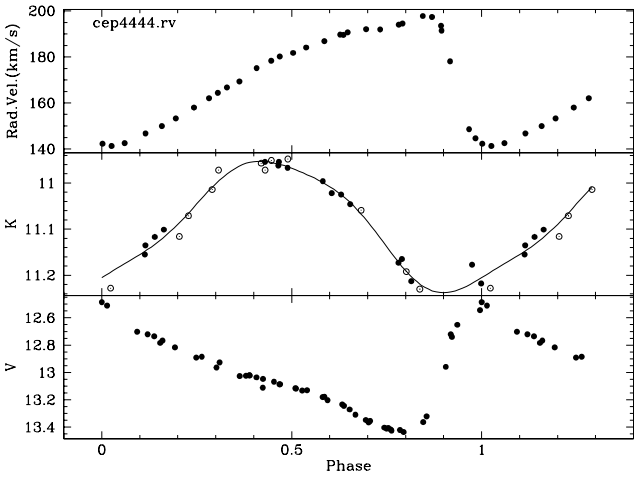

Fig. A.26. Light and radial velocity curves for the star OGLE-SMC-CEP4444.

be seen that the offsets follow a slow secular change compared to the pulsational periods. For two of the suspected binary stars, OGLE-SMC-CEP-1686 and -1693 we did not find good shifts. In the first case the offsets were small so we simply adopted the data as they were observed. For the second star, however, the offsets seemed to be very large compared to the pulsational amplitude and the timescale also seemed to be comparable to the pulsational period. We consider this star to be peculiar and disregarded it in the further analysis. The velocity offsets as well as the corrected velocities for the five stars can be found in Table B.1.

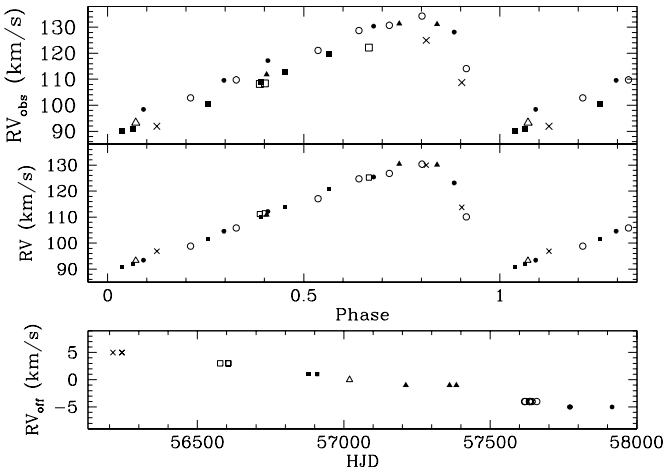

Fig. B.1. Observed radial velocities for the star OGLE-SMC-CEP-1680 are shown in the *upper panel*. In the *middle panel* the adopted velocities are shown after applying radial velocity offsets to the data from a given epoch. The velocity offsets adopted are shown as a function of time in the *lower panel*. Different symbols refer to different epochs.

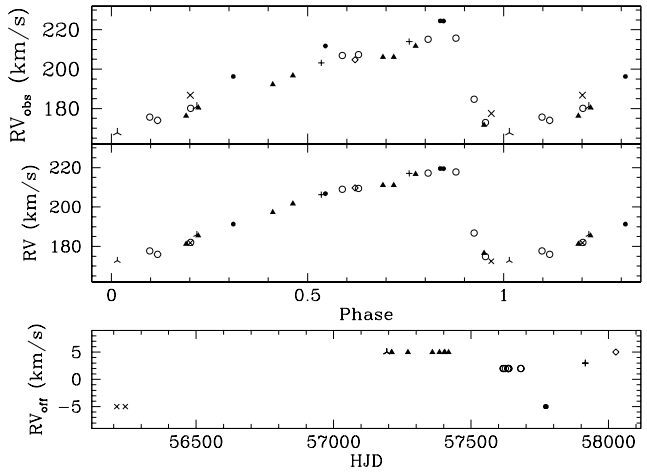

Fig. B.2. Observed radial velocities for the star OGLE-SMC-CEP-1729 are shown in the *upper panel*. In the *middle panel* the adopted velocities are shown after applying radial velocity offsets to the data from a given epoch. The velocity offsets adopted are shown as a function of time in the *lower panel*. Different symbols refer to different epochs.

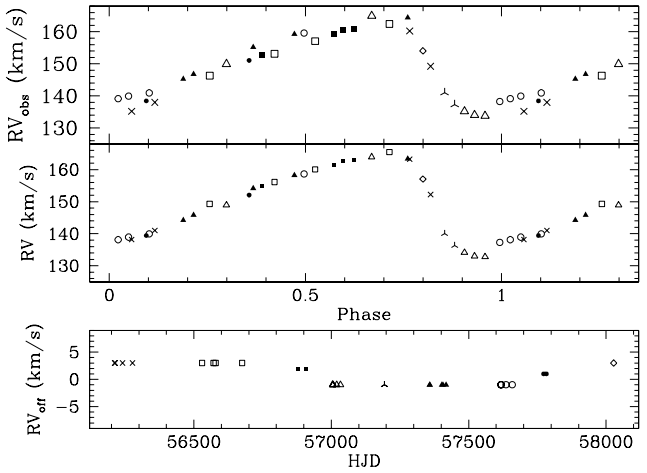

Fig. B.4. Observed radial velocities for the star OGLE-SMC-CEP-2905 are shown in the *upper panel*. In the *middle panel* the adopted velocities are shown after applying radial velocity offsets to the data from a given epoch. The velocity offsets adopted are shown as a function of time in the *lower panel*. Different symbols refer to different epochs.

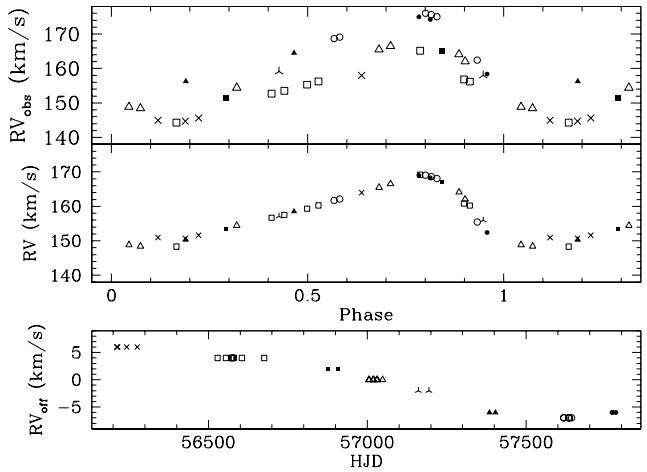

Fig. B.3. Observed radial velocities for the star OGLE-SMC-CEP-1977 are shown in the *upper panel*. In the *middle panel* the adopted velocities are shown after applying radial velocity offsets to the data from a given epoch. The velocity offsets adopted are shown as a function of time in the *lower panel*. Different symbols refer to different epochs.

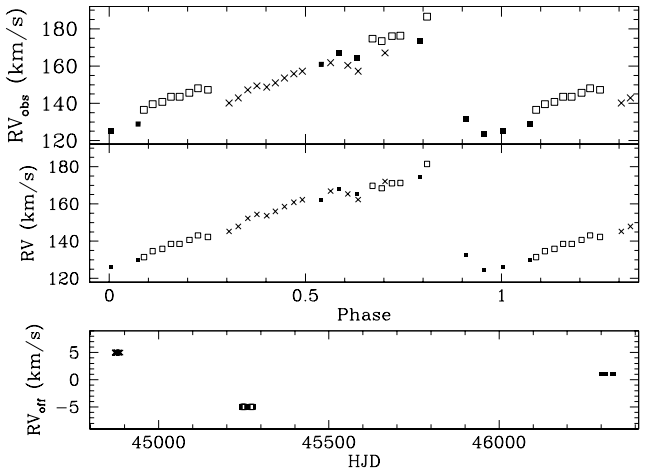

Fig. B.5. Observed radial velocities for the star HV 837 are shown in the *upper panel*. In the *middle panel* the adopted velocities are shown after applying radial velocity offsets to the data from a given epoch. The velocity offsets adopted are shown as a function of time in the *lower panel*. Different symbols refer to different epochs.

Table B.1. Radial velocities, *RV*, corrected for the putative orbital motion.

Identifier	phase	HJD	RV_{obs}	σ	RV	RV_{off}
OGLE-SMC-CEP-1680	0.038	2456877.71500	89.99	0.37	90.99	1.0
OGLE-SMC-CEP-1680	0.064	2456877.84320	91.02	0.40	92.02	1.0
OGLE-SMC-CEP-1680	0.072	2457019.64830	93.30	0.08	93.30	0.0
OGLE-SMC-CEP-1680	0.091	2457772.57380	98.44	0.07	93.44	−5.0
OGLE-SMC-CEP-1680	0.126	2456242.63810	91.89	0.41	96.89	5.0
OGLE-SMC-CEP-1680	0.212	2457616.72960	102.84	0.50	98.84	−4.0
OGLE-SMC-CEP-1680	0.256	2456878.77960	100.66	0.22	101.66	1.0
OGLE-SMC-CEP-1680	0.297	2457773.57740	109.59	0.06	104.59	−5.0
OGLE-SMC-CEP-1680	0.328	2457636.85270	109.78	0.34	105.78	−4.0
OGLE-SMC-CEP-1680	0.388	2456605.67110	108.20	0.30	111.20	3.0
...						
		days	km s^{-1}	km s^{-1}	km s^{-1}	km s^{-1}

Notes. Listed are the identifier; the pulsational phase; the HJD; the actually observed radial velocity, RV_{obs}; the estimated statistical uncertainty, σ; the corrected radial velocity, *RV*; and the applied velocity offset, RV_{off}. The full table is available at CDS.